

3

Formulations éléments finis généralisées pour la vibro-acoustique

Quand un bruit vous ennuie, écoutez-le.

(John Cage)

3.1 Méthode de partition de l'unité (PUM)

3.1.1 Qu'est-ce qu'une méthode de partition de l'unité ?

La méthode de partition de l'unité a été proposée par I. Babuška *et al.* [BAB97b] et illustrée principalement sur l'équation de Laplace ou de l'élasticité (avec singularités), sur l'équation de Helmholtz (à 1D toutefois) et sur une classe générale de problèmes elliptiques. L'originalité majeure de la méthode consistait à conserver un partitionnement de type éléments finis du domaine mais de formuler la méthode d'approximation de telle manière que l'on puisse incorporer facilement des informations locales sur la solution. La méthode *hp-clouds* proposée simultanément par J. T. Oden [ODE96] ou, plus récemment, celle de T. Belytschko appelée X-FEM [MOE99], peuvent être vues comme des méthodes PUM. Depuis lors, T. Strouboulis a présenté une méthode des éléments généralisée basée principalement sur PUM mais offrant en outre la possibilité d'utiliser des maillages indépendants de la géométrie [STR00, STR01a, STR01b]. Dans le cadre de ce travail toutefois, nous nous baserons sur la version initiale de la méthode PUM [BAB97b].

La méthode de partition de l'unité est basée principalement sur l'idée de toujours considérer des fonctions qui partitionnent l'unité en tout point du domaine. Considérons un ensemble de fonctions N_i et un domaine Ω recouvert par un ensemble de domaines ouverts Ω_i (appelés *patches*) tels que :

$$\begin{aligned} \text{supp}(N_i) &= \Omega_i \\ \forall \mathbf{x} \in \Omega, \sum_i N_i &= 1 \end{aligned} \tag{3.1}$$

où $\text{supp}(N_i)$ désigne le support (domaine de définition) de la fonction N_i . Considérons encore l'espace de fonctions V_i^P définies sur Ω_i . Dans ce cas, l'espace de fonctions utilisé pour l'approximation est

$$V = \text{span}\{N_i v_i^P\} \quad \text{avec } v_i^P \in V_i^P \tag{3.2}$$

où $\text{span}\{N_i v_i^P\}$ désigne l'espace des fonctions engendrées par l'ensemble des fonctions $N_i v_i^P$.

Chaque nœud a plusieurs degrés de liberté (un par fonction de V_i^P) et l'approximation d'une fonction u au point \mathbf{x} est donnée par

$$u^h(\mathbf{x}) = \sum_i \sum_{v_i^P \in V_i^P} a_{i,p} N_i v_i^P(\mathbf{x}) \quad (3.3)$$

Les coefficients $a_{i,p}$ sont les inconnues et ils sont déterminés à l'aide d'une méthode de collocation ou bien à l'aide de la méthode de Galerkin. Dans la suite, les fonctions N_i seront toujours choisies parmi les fonctions éléments finis et les fonctions v_i^P font l'objet de l'étude par la prise en considération d'information locale sur la solution.

3.1.2 Application aux plaques de Kirchhoff

Avant d'aborder les problèmes vibro-acoustiques couplés 3D, il est nécessaire de disposer d'une formulation enrichie pour les plaques et les coques. Dans ce cadre, nous avons tout d'abord montré qu'il était possible de formuler une méthode de partition de l'unité pour les poutres que nous avons couplée à un domaine fluide 2D [DEB02, BOU04]. Ensuite, nous avons formulé cette méthode pour l'étude des vibrations harmoniques d'une plaque mince, sous les hypothèses cinématiques de Kirchhoff (les sections planes restent planes après déformation). Dans ce cas, les déplacements transversaux de la plaque sont régis par l'équation différentielle du quatrième ordre suivante :

$$D(\nabla^4 w(x, y) - k_b^4 w(x, y)) = F \quad (3.4)$$

où

$$k_b = \sqrt[4]{\frac{\rho_s e \omega^2}{D}} ; D = \frac{E e^3 (1 + j\eta)}{12(1 - \nu^2)} \quad (3.5)$$

Les solutions de l'équation homogène associée à (3.4) peuvent s'exprimer sous la forme d'une série infinie :

$$w^h(x, y) = \sum_{s=1}^{\infty} w_s \Psi_s(x, y) \quad (3.6)$$

dont les solutions oscillantes sont données par

$$\begin{cases} \Psi_s(x, y) = e^{-j(k_{x,s}x + k_{y,s}y)} \\ (k_{x,s}^2 + k_{y,s}^2)^2 = k_b^4 \end{cases} \quad (3.7)$$

La solution de l'équation (3.4) pour une fréquence donnée correspond donc à la superposition d'une infinité de termes exponentiels (vecteur tournant de rayon k_b) dont w_s définit l'amplitude.

L'utilisation d'une méthode PUM n'est pas directement possible dans la mesure où il faudrait introduire une infinité de termes dans la base correspondant aux différentes valeurs $s=0,1,2,\dots$ de l'équation (3.6).

Afin de pouvoir utiliser la méthode PUM, il est toutefois possible de réduire le nombre de termes dans la base. Pour ce faire, nous adoptons 3 hypothèses simplificatrices :

- 1) à moyenne fréquence, on peut négliger les termes imaginaires qui interviennent dans la solution (3.6). Ceci permet de réduire l'espace des fonctions aux seuls termes réels :

$$w^h(x,y) = \text{span} \left\{ \begin{array}{l} \sin(k_{x,s}x)\sin(k_{y,s}y); \sin(k_{x,s}x)\cos(k_{y,s}y); \\ \cos(\dots)\sin(\dots); \cos(\dots)\cos(\dots) \end{array} \right\} \quad (3.8)$$

- 2) on considère la propagation de l'onde suivant des angles θ_s . Il existe une relation entre k_b et $k_{x,s}$, $k_{y,s}$, θ_s :

$$\begin{cases} k_{x,s} = k_b \cos \theta_s \\ k_{y,s} = k_b \sin \theta_s \end{cases} \quad (3.9)$$

- 3) en chaque point de la plaque, il est possible d'exprimer un angle de propagation local unique $\theta_s = \theta(x,y)$. La base devient alors

$$w^h(x,y) = \text{span} \left\{ \begin{array}{l} \sin(k_x(x,y)x)\sin(k_y(x,y)y); \sin(\dots)\cos(\dots); \\ \cos(\dots)\sin(\dots); \cos(\dots)\cos(\dots) \end{array} \right\} \quad (3.10)$$

Ne connaissant pas *a priori* la valeur de θ en chaque point, nous optons pour une méthode itérative analogue à celle que nous avons proposée pour l'acoustique [LAC03]. Un premier calcul est effectué avec une base polynomiale, ou, si on veut améliorer la précision de la première itération, avec une base contenant des termes sinus et cosinus d'angles de propagation arbitraires.

Une fois la première solution w^h_1 , obtenue, il faut déterminer l'angle de propagation local en chaque nœud. Ceci est rendu possible à l'aide d'une transformée de Fourier rapide (FFT) de la solution sur une cellule contenant le nœud considéré. À l'aide d'un échantillon de valeurs w^h_1 , dans la cellule du nœud i , la méthode FFT nous renseigne sur les valeurs k_x et k_y au nœud i et donc sur l'angle de propagation. Cet angle de propagation sera utilisé comme angle à la deuxième itération pour la base locale associée au nœud i . Des angles secondaires seront éventuellement également présents dans la base (uniformément répartis autour de l'angle principal) afin d'obtenir une convergence rapide de la solution.

Les itérations s'arrêtent lorsqu'en chaque nœud la valeur de l'angle de propagation ne varie plus (à une tolérance donnée) et lorsque la solution w_h obtenue à l'itération $i-1$ est la même (à une tolérance donnée) que celle obtenue à l'itération i . Cette double condition de convergence est nécessaire car, pour les fréquences proches d'une fréquence propre, une faible variation d'angle peut engendrer un écart important entre les solutions w^h_{i-1} et w^h_i .

L'article qui suit présente la formulation proposée pour la vibration d'une plaque de Kirchhoff en l'absence d'amortissement ainsi que la manière dont nous avons abordé les aspects numériques propres à ce genre de méthodes (conditions aux limites de Dirichlet, intégration numérique). Un test a été réalisé sur une plaque carrée pour laquelle une solution éléments finis est comparée à une solution PUM à base polynomiale ou à base locale calculée.

L'article est un preprint de E. De Bel, P. Villon, Ph. Bouillard, 'Forced vibrations in the medium frequency range solved by a partition of unity method with local information', Int. j. numer. methods eng. 2004, *in press*.

INTERNATIONAL JOURNAL FOR NUMERICAL METHODS IN ENGINEERING
Int. j. numer. methods eng. 2004, *in press*

Forced vibrations in the medium frequency range solved by a partition of unity method with local information

E. De Bel¹, P. Villon² and Ph. Bouillard^{1,*}

¹*Department of Structural and Material Computational Mechanics*

Université Libre de Bruxelles, F.D. Roosevelt Av., 50, CP 194/5 – Brussels, Belgium

²*Centre de Recherche de Royallieu, Génie des Systèmes Mécaniques BP 20529
 60205 Compiègne Cédex, France*

SUMMARY

A new approach for the computation of the forced vibrations up to the medium frequency range is formulated for thin plates. It is based on the Partition of Unity Method (PUM), first proposed by I. Babuška, and used here to solve the elastodynamic problem. The paper focuses on the introduction of local information in the basis of the Partition of Unity Method coming from previous approximations, in order to enhance the accuracy of the solution. The method may be iterative and generates a PUM approximation leading to smaller models compared with the finite element ones required for a same accuracy level. It shows very promising results, in terms of frequency range, accuracy and computational time.

KEY WORDS : elastodynamics, vibrations, partition of unity method, medium frequency, plate

1. INTRODUCTION

During the last few years, the vibration and acoustical aspects of mechanical problems have gradually acquired a significant importance in industrial modelling processes, especially in the automotive and aeronautical fields. For the low frequency range, finite element (FEM) and boundary element (BEM) are still the most widely used methods to solve wave propagation problems, even for complex structures. On the other hand, for high frequencies, other techniques are developed where the spatial aspect disappears almost entirely: Statistical Energy Analysis (SEA) methods for instance.

Despite considerable recent efforts to extend the possibly frequency range of both the FE and the SEA methods, there are no fully satisfactory numerical procedures to cover the medium frequency range. The key issue to improve the accuracy of the approximate numerical solution, or, alternatively, to simulate properly the medium frequency range, for wave propagation in bounded domains, or for near-field sub-domains in unbounded domains, is to control the dispersion error [1-2]. It is particularly crucial for industrial purpose, where robust methods are necessary for the medium frequency range within a reasonable computational cost, or sufficiently accurate numerical models to enable updating with experimental data [3]. High order approximations have then been proposed based on the finite element method (*hp* formulations [4-5]) where shape functions are better suited to wave propagation, or on meshless methods [6-9] where shape functions are non-rational and can contain *a priori* known terms in

* Correspondence to: Ph. Bouillard, Université Libre de Bruxelles, Structural and Material Computational Mechanics Dept. CP 194/5, F.D. Roosevelt Av. 50, B-1050 Brussels, Belgium. E-mail: Philippe.Bouillard@ulb.ac.be

Contract/grant sponsor: Région Wallonne

Contract/grant sponsor: Commissariat général aux Relations internationales (CGRI)

Received 17 September 2003
 Revised 21 June 2004

the basis of approximation. Today, everybody seems to agree that it is even more advantageous to incorporate information on the solution itself into the numerical discrete subspace, see for instance the wave envelope approach [10], the Discontinuous Galerkin FEM [11-13], the Trefftz based approach [14], or the Variational Theory of Complex Rays [15].

In the present paper, we will focus on the forced vibrations of thin plates for which some already mentioned methods have also been formulated [16-17]. In the case of plates or shells, numerical issues appear however when using meshless methods or Trefftz based approaches because they do not have an element discretisation of the domain at their disposal [18-19].

Based on previous work [20-22], we suggest to use a generalised FEM based on the Partition of Unity Method (PUM), first proposed by I. Babuška [23], formulated for the elastodynamics. This solution allows us to keep finite element discretisation and thus to have an easy description of the topology for numerical integration purpose. As many other formulations, the PUM leads to the exact solution for trusses of bars or beams [20]. In the case of plates however, the exact solution cannot be numerically obtained since it would require an infinite number of terms in the basis. This is the reason why the PUM approximation is restricted in this paper to only a small set of these terms, which are chosen with the help of local information about the vibration of the plate, coming from a previous computation.

Unfortunately, some drawbacks arise with the use of this technique, such as frequency-dependent matrices or large number degrees of freedom per node, but this paper aims at the demonstration that this method has cheaper computational costs for the medium frequency range than classical FE or high order approximation.

The paper is organised as follows : Section 2 recalls the basics of the PUM and explains how it can be formulated for the elastodynamic analysis of a thin plate. Section 3 describes how the method can further be improved by computing the wave propagation angle locally and enrich the basis with this result. Section 4 addresses two classical numerical issues of these formulations (the Dirichlet boundary conditions and the numerical quadrature). Section 5 is dedicated to the analysis of the performances of the method in terms of convergence, frequency limit and computational time. Finally, Section 6 gives the conclusions.

2. PARTITION OF UNITY METHOD APPLIED TO PLATES IN ELASTODYNAMICS

2.1. Introduction

The Partition of Unity method [23] can be seen as a generalised finite element method where the core ideas are, first, the construction of the spaces with local approximation properties and, second, the conformity of these spaces. A feature of those spaces is that it can approximate the exact solution well locally. When the exact solution of a problem can be expressed, the PUM can give very accurate results [24]. If it is not the case, the introduction of others functions in the space looks like a p -refinement of the finite element solution. For a thorough analysis of the design and the selection of shape functions in the generalised finite element method, see References [28-31].

The main advantages of the PUM are :

- the introduction of *a priori* known terms in the basis V is possible ;
- the shape functions are easily computed in comparison with other p -methods ;
- spaces of any desired regularity can be constructed. Therefore, the *test* functions needed in the variational formulations of high order differential equations (such as beam, plates and shell problems) become available.
- local refinement is easily computed by modifying the functions in the appropriate subspaces.

However, major drawbacks remain :

- the numerical integration of high order functions requires appropriate schemes
- the continuity of the displacement field of non coplanar shells requires a specific attention. In a PUM, it is even more necessary since the unknowns are not the displacement components but the coefficients of the basis expansion.

In this paper, the PUM is formulated with a local enrichment of the basis based on the exact solution of the elastodynamic problem. The terms of the exact solution of the homogeneous problem are expressed in the local basis everywhere since the pollution error of a wave propagation approximation is global [2].

2.2. Basics of the PUM

The foundations of the PUM consist in partitioning the unity. Consider a set of functions N_i and a domain Ω overlapped by a set of open domains Ω_i , the so-called *patches*, such as :

$$\begin{aligned} \text{supp}(N_i) &= \Omega_i \\ \forall x \in \Omega, \sum_i N_i &= 1 \end{aligned} \quad (1)$$

where $\text{supp}(N_i)$ denotes the support of definition of the function N_i .

The N_i compose the partition of unity attached to the patch Ω_i . Consider now the space of functions V_i^p defined on Ω_i . In this case, the space of functions used for the approximation is

$$v = \text{span}\{N_i V_i^p\} \text{ with } V_i^p \in v_i^p \quad (2)$$

where $\text{span}\{N_i V_i^p\}$ denotes the space of functions generated by the set of functions $N_i V_i^p$.

Each node has several degrees of freedom (one per function of V_i^p) and the approximation of a function at the point x is given by :

$$u^h(x) = \sum_i \sum_{V_i^p \in v_i^p} a_{i,p} N_i V_i^p(x) = \sum_i \{\Phi_i(x)\}^t \{A\}_i \quad (3)$$

The $a_{i,p}$ are the unknown coefficients and they can be computed either by a collocation method or by a Galerkin method. To formulate the PUM as an enriched FEM, one has to correctly choose the patches Ω_i . For plate problems, for instance, the patch contains adjacent finite elements (the patches Ω_i are overlapping) and the functions N_i can be the usual functions of the finite element method (see Figure 1).

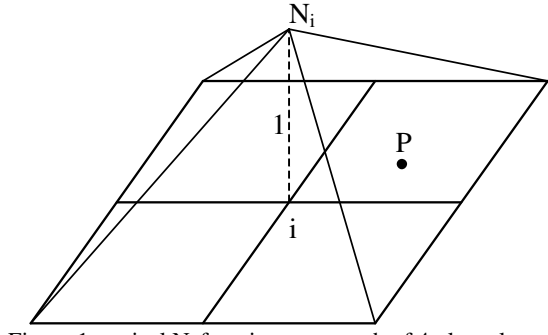


Figure 1. typical N_i function on a patch of 4 plate elements

2.3. Appropriate PUM basis for the structural dynamics of thin plates

In order to construct appropriate shape functions for the structural dynamics, it is necessary to address the problem and to discuss the analytical solution available for the corresponding homogenous problem. According to the thin plate theory [25], the steady-state out-of-plane displacement $w(x,y)$ is governed by the following differential equation :

$$D(\nabla^4 w(x,y) - k_b^4 w(x,y)) = F(x,y) \quad (4)$$

where $\nabla^4 = \frac{\partial^4}{\partial x^4} + 2\frac{\partial^4}{\partial x^2 \partial y^2} + \frac{\partial^4}{\partial y^4}$. The plate bending wavenumber k_b and the plate bending stiffness D

are given by

$$k_b = \sqrt[4]{\frac{\rho_s e \omega^2}{D}} , \quad D = \frac{E e^3 (1+j\eta)}{12(1-\nu^2)} \quad (5)$$

where e , E , ν , ρ_s , η and ω are the plate thickness, the Young modulus, the Poisson coefficient, the material mass density, the damping factor and the pulsation, respectively.

The exact homogenous solution $w^h(x,y)$ of differential equation (4) can be seen as an infinite expansion given by

$$w^h(x,y) = \sum_{s=1}^{\infty} w_s \Psi_s(x,y) \quad (6)$$

where the functions $\Psi_s(x,y)$ are defined by

$$\Psi_s(x,y) = e^{-j(k_{x,s}x+k_{y,s}y)} \quad (7)$$

with

$$(k_{x,s}^2 + k_{y,s}^2)^2 = k_b^4 \quad (8)$$

Previous works [20] have proved that the introduction of the entire set of functions coming from the homogenous solution into the partition of unity method allows to obtain the exact solution on the whole domain. In the present work, the introduction of all the functions composing the homogenous solution is not possible anymore, because an infinite number of terms can obviously not be incorporated in the basis. Further assumptions have to be made.

2.4. Further assumptions to build the PUM basis

The choice of functions to build the basis must be restricted. The following simplifications are assumed: the imaginary part of the out-of-plane displacement is neglected. This assumption becomes more and more acceptable as the frequency grows. This simplification reduces the basis of functions to the real terms only:

$$w^h(x,y) = \text{span} \left\{ \sin(k_{x,s}x)\sin(k_{y,s}y), \sin(k_{x,s}x)\cos(k_{y,s}y), \cos(k_{x,s}x)\sin(k_{y,s}y), \cos(k_{x,s}x)\cos(k_{y,s}y) \right\} \quad (9)$$

as a consequence of the first assumption, equation (8) leads to

$$\begin{cases} k_{x,s} = k_b \cos \theta_s \\ k_{y,s} = k_b \sin \theta_s \end{cases} \quad (10)$$

where θ_s is a local wave propagation angle.

However, an infinite number of terms still exists in the basis, each defined by a specific wave propagation angle (different values of s). The next simplification consists in truncating the number of

wave propagation angles at each point of the plate: in each point x and y of the plate, one wave propagation angle $\theta(x,y)$ can be assumed.

Hence, the set of function becomes :

$$\theta_s = \theta(x, y) \quad (11)$$

↓

$$\begin{cases} k_x(x, y) = k_b \cos \theta(x, y) \\ k_y(x, y) = k_b \sin \theta(x, y) \end{cases} \quad (12)$$

↓

$$w^h(x, y) = \text{span} \left\{ \begin{array}{l} \sin(k_x(x, y)x) \sin(k_y(x, y)y) \\ \sin(k_x(x, y)x) \cos(k_y(x, y)y) \\ \cos(k_x(x, y)x) \sin(k_y(x, y)y) \\ \cos(k_x(x, y)x) \cos(k_y(x, y)y) \end{array} \right\} \quad (13)$$

Because the patches contain a part of the plate domain, and because the space of function V is defined on each patch, different orientations of θ will be taken in the space of function. Otherwise, the wave propagation angle will be constant by patch.

Since the values of the wave propagation angle $\theta(x,y)$ are not known *a priori*, an iterative method for adapting the wave propagation angle at each computation is proposed. For a fast convergence, the terms $\{I, x, y\}$ enrich the basis.

2.5. Discretised equations of the undamped elastodynamics

The discretisation of the undamped elastodynamic system for a plate (eq. 4) is described below :

$$([K] - \omega^2 [M])\{q\} = \{F\} \quad (14)$$

with

$$[K] = \sum_{e=\text{element}} [k]_e \quad ; \quad [M] = \sum_{e=\text{element}} [m]_e \quad ; \quad \{q\} = \sum_{e=\text{element}} \{q\}_e \quad ; \quad \{F\} = \sum_{e=\text{element}} \{f\}_e \quad (15)$$

and

$$[k]_e = \begin{bmatrix} [0] & [0] \\ [0] & [k_f] \end{bmatrix} + [k_c] \quad (16)$$

$$[m]_e = \begin{bmatrix} [0] & [0] \\ [0] & [m_f] \end{bmatrix} + [m_c] \quad (17)$$

$$\{q\}_e = \left\{ \begin{array}{l} \{A^w\}_e \\ \{A^{\beta_x}\}_e \\ \{A^{\beta_y}\}_e \end{array} \right\} \quad (18)$$

$$\{f\}_e^t = \left\{ \begin{array}{l} \{f_w\} \quad \{f_{\beta_x}\} \quad \{f_{\beta_y}\} \end{array} \right\} \quad (19)$$

$[k_f]$ and $[k_c]$ are the bending stiffness and the shear stiffness matrix respectively. They are defined by:

$$[k_f] = \int_{\Omega} [B_f]^t [H_f] [B_f] d\Omega \quad (20)$$

$$[k_c] = \int_{\Omega} [B_c]^t [H_c] [B_c] d\Omega \quad (21)$$

in which $[H_f]$ and $[H_c]$ are the bending and the shear Hooke matrices :

$$[H_f] = \frac{Eh^3}{1-\nu^2} \begin{bmatrix} 1 & \nu & 0 \\ \nu & 1 & 0 \\ 0 & 0 & \frac{1-\nu}{2} \end{bmatrix} \quad (22)$$

$$[H_c] = Gkh \begin{bmatrix} 1 & 0 \\ 0 & 1 \end{bmatrix} \quad (k : \text{shear correction factor} ; G : \text{shear modulus}) \quad (23)$$

and $[B_f]$ and $[B_c]$ are the derivatives of the shape functions expressed by :

$$[B_f] = \begin{bmatrix} \left\langle \frac{\partial \Phi^{\beta_x}}{\partial x} \right\rangle & \langle 0 \rangle \\ \langle 0 \rangle & \left\langle \frac{\partial \Phi^{\beta_y}}{\partial y} \right\rangle \\ \left\langle \frac{\partial \Phi^{\beta_x}}{\partial x} \right\rangle & \left\langle \frac{\partial \Phi^{\beta_y}}{\partial y} \right\rangle \end{bmatrix} \quad \text{and} \quad [B_c] = \begin{bmatrix} \left\langle \frac{\partial \Phi^w}{\partial x} \right\rangle & \left\langle \Phi^{\beta_x} \right\rangle & \langle 0 \rangle \\ \left\langle \frac{\partial \Phi^w}{\partial y} \right\rangle & \langle 0 \rangle & \left\langle \Phi^{\beta_y} \right\rangle \end{bmatrix} \quad (24)$$

$\langle \Phi^w \rangle$, $\langle \Phi^{\beta_x} \rangle$ and $\langle \Phi^{\beta_y} \rangle$ are the shape function of respectively the out-of-plane displacement w , the rotation along the x -axis and the rotation along the y -axis (x -axis and y -axis are the local element axis). These shape functions are used for the PUM approximations of the three different fields (see equation 3) and they contain the basis V^w , V^{β_x} and V^{β_y} :

$$\begin{cases} w^h(x, y) = \sum_i \{\Phi^w\}_i \{A^w\} \\ \beta_x^h(x, y) = \sum_i \{\Phi^{\beta_x}\}_i \{A^{\beta_x}\} \\ \beta_y^h(x, y) = \sum_i \{\Phi^{\beta_y}\}_i \{A^{\beta_y}\} \end{cases} \quad \text{with} \quad \begin{cases} \langle \Phi^w \rangle = \langle \langle N_1 V_{11}^w \dots N_1 V_{1m}^w \rangle \dots \langle N_n V_{n1}^w \dots N_n V_{nm}^w \rangle \rangle \\ \langle \Phi^{\beta_x} \rangle = \langle \langle N_1 V_{11}^{\beta_x} \dots N_1 V_{1m}^{\beta_x} \rangle \dots \langle N_n V_{n1}^{\beta_x} \dots N_n V_{nm}^{\beta_x} \rangle \rangle \\ \langle \Phi^{\beta_y} \rangle = \langle \langle N_1 V_{11}^{\beta_y} \dots N_1 V_{1m}^{\beta_y} \rangle \dots \langle N_n V_{n1}^{\beta_y} \dots N_n V_{nm}^{\beta_y} \rangle \rangle \end{cases} \quad (25)$$

where n is the number of nodes of the element and m is the number of terms defining the basis V^w , V^{β_x} or V^{β_y} (the same terms are used for each different approximation).

2.6. Number of degrees of freedom in the PUM approximation

Now that the choice of the terms composing the bases is achieved and that the three approximation fields are defined, it is easy to count the number of degrees of freedom per node :

$$\text{Number of d.o.f.'s per node} = 3 * (3 + 4 * T) \quad (26)$$

This number corresponds to the number of fields to approximate (w , β_x and β_y) multiplied by the number of terms in the basis : $\{I, x, y\}$ and 4 trigonometric terms for each angle of propagation (T

represents the number of angles taken for the approximation). If one angle of propagation is used, 21 degrees of freedom per node will be necessary, for two angles, 33, etc.

3. THE ITERATIVE SCHEME

This section explains the methodology of the new proposed iterative method in detail and is illustrated by the example of a thin aluminium plate in free vibrations (figure 2).

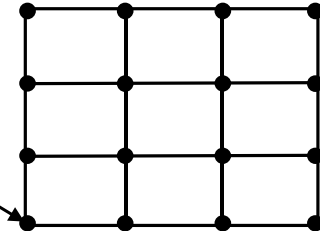


Figure 2. 3x3 discretisation of a plate of $0.4m \times 0.3m$ - thickness = 1,5mm
excitation 1000Hz at the corner
3 angles of propagation are considered = $3 * (3 + 4*3) * 16$ nodes = 720 dofs.

A first solution of the problem with initial values of propagation angle is required to give a first approximation of the out-of-plane displacement field w_i^h . The next steps follow the iterative scheme given in figure 3 until the convergence over θ and w^h is achieved.

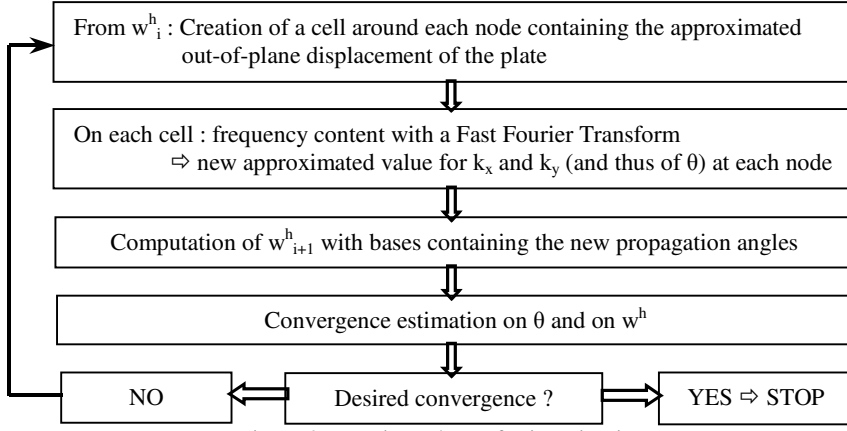


Figure 3. Iterative scheme for iteration i

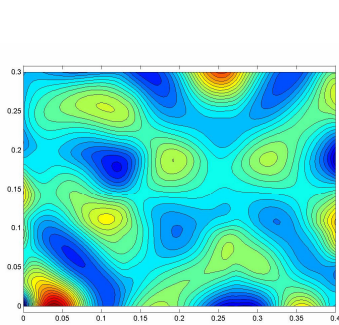


Figure 4. Deformed plate at 1000Hz – first iterate

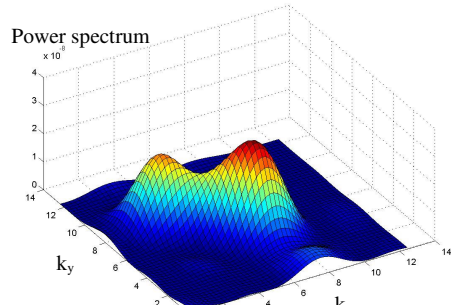


Figure 5. Frequency content of cell 1

In this example, the three initial angles are 15° , 45° and 75° (angles are always in the first quadrant with regards to the terms composing the basis) and a first computation of w^h with these angles gives a

deformed plate shown in figure 4. From a FFT analysis of the cell of the node 1, of coordinates (0,0), the power spectrum function of k_x and k_y is presented in figure 5.

It is interesting to observe that the maximum is located on an arc with a radius k_b (see figure 6). The propagation angle for node 1 at iteration 2 is determined by the root extraction of the derivative of a 20th order polynomial fitting the power spectrum on this arc of radius k_b (figure 7).

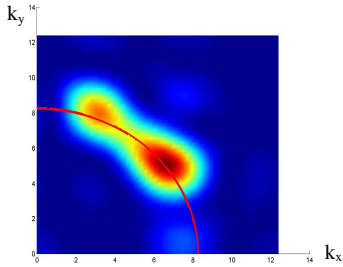


Figure 6. Frequency content and arc of radius k_b

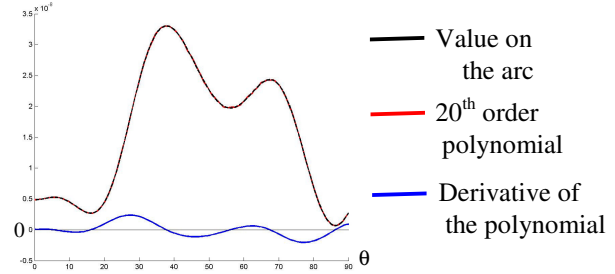


Figure 7. Polynomial fitting the power on the arc

A similar FFT analysis is performed on all the nodes giving the new bases containing new propagation angle and then the next iteration can be executed. The iteration scheme stops when there is no variation left over θ and over w^h (i.e. when the error stands below a prescribed tolerance). The convergence over θ and over w^h is expressed by the following norms:

$$\text{Convergence over } \theta = \frac{\|\theta_i - \theta_{i-1}\|}{\|\theta_i\|} \quad (27)$$

$$\text{Convergence over } w^h = \frac{\int_{\Omega} (w_i^h - w_{i-1}^h) d\Omega}{\int_{\Omega} (w_i^h) d\Omega} \quad (28)$$

where θ_i is a vector containing the values of the propagation angle at each node for iteration i .

Table 1 shows the next iterations of the free plate example.

Five iterations are sufficient to obtain a good approximation of the plate at 1000Hz in comparison with the reference (ACTRAN® FE mesh with 136.806 dofs). For this frequency, a fast convergence is observed over the propagation angle which is not really the case for the convergence over w^h . The reason for this behaviour is that the computational frequency is close to an eigenfrequency (996 Hz), so that a little difference over the propagation angle leads to significant different displacements of the plate. Between two distinct eigenfrequencies, this problem does not appear and a maximum of 2 or 3 iterations are needed.

Another interesting point is that above a certain frequency there is no convergence any longer for a considered discretisation of the plate. This results from a too coarse discretisation with respect to the frequency. A refinement of the mesh is then necessary, in order to have a larger number of nodes which will better capture the variation of the propagation angle.

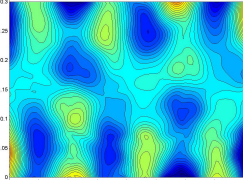
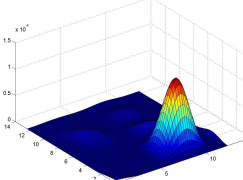
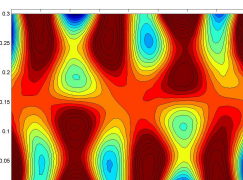
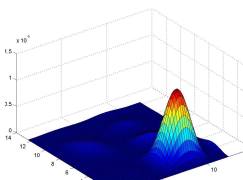
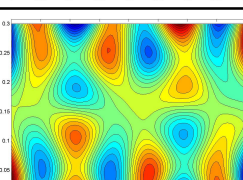
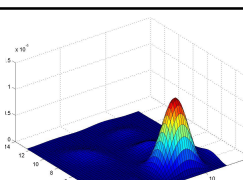
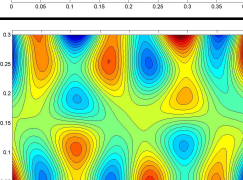
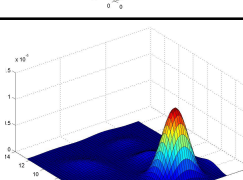
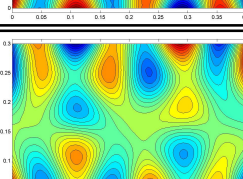
Iteration	w^h	Frequency content of node 1	θ at node 1	Convergence over θ	Convergence over w^h
2			15,1°	0,479	0,925
3			14,715°	0,0138	0,839
4			14,732°	5,16 10 ⁻⁴	0,517
5			14,731°	1,74 10 ⁻⁵	0,0479
Reference					

 Table 1. w^h and the convergences over θ and w^h of the free plate example

4. FURTHER NUMERICAL ISSUES

4.1 Dirichlet boundary condition

4.1.1 *Different formulations to apply the Dirichlet boundary conditions.* In a PUM, the degrees of freedom are the unknown coefficients of expansion (3). Additional techniques should then be used to enforce the essential boundary conditions. There exist several ways to impose the essential boundary, depending on the type of conditions.

If only a component of a nodal displacement has to be prescribed, it is sufficient to modify the terms in the PUM basis in this node only [23]. The PUM degenerates there in a classical finite element approximation by only keeping in the basis V_i^P the singleton term {1}. If the displacement at node i , for instance, has to be prescribed, the following basis is used:

$$w_i^h(x, y) = \text{span} \left\{ 1, (x - x_i), (y - y_i), (\sin(k_{x1}x)\sin(k_{y1}y) - \sin(k_{x1}x_i)\sin(k_{y1}y_i)), \dots \right\} \quad (29)$$

Prescribing a linear constraint on an edge, or between two nodes, is not so simple in PUM. In a finite element formulation, it is sufficient to prescribe the nodal values to obtain a linear displacement (since the shape functions can represent exactly a linear function). In the PUM, linear shape functions are not preserved by using bases in (29) (see Figure 8b, the transverse displacement is prescribed to zero in nodes 1, 2 and 3).

A first natural idea consists of the generalisation of the previous one: the PUM can degenerate in a finite element formulation on an edge. The terms of the basis are multiplied by a function that vanishes on the prescribed edge. This function is directly derived from the equation of the edge. The shape function becomes the classical finite element one, similar to figure 1, and the essential boundary conditions can be imposed directly as in FEM. Using this method, figure 8(c) shows that the plate has a linear displacement between nodes at the corner which is not the case in figure 8(b), where only the three nodal values are prescribed using (29).

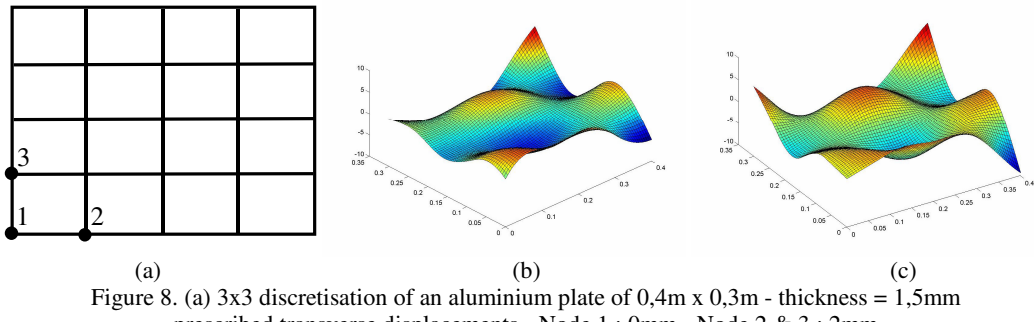


Figure 8. (a) 3x3 discretisation of an aluminium plate of 0,4m x 0,3m - thickness = 1,5mm
prescribed transverse displacements - Node 1 : 0mm - Node 2 & 3 : 2mm
(b) displacement prescribed at the nodes only (500Hz)
(c) displacement prescribed at the nodes interpolated with linear shape functions (500Hz)

This methodology is not the simplest, but the use of Lagrange multipliers is avoided. This allows us to remain with a system to be solved with no additional degrees of freedom and also to use efficient resolution methods.

In order to be very general, one has also to deal with complex boundary conditions. It is not the purpose of the paper to develop original ideas on boundary conditions. It is then suggested to adopt a weak penalty method as proposed in [26]. It consists in a modification of the variational form itself by adding a term corresponding to the essential boundary conditions. In the present case, the variational problem becomes:

$$\int_{\Omega_s} \sigma^t(u) \varepsilon(\delta u) d\Omega + \int_{\Omega_s} \rho \frac{\partial^2 u}{\partial t^2} \delta u d\Omega + \int_{\Gamma_u} (u - \bar{u})^t \alpha (\delta u - \delta \bar{u}) d\Gamma - \int_{\Gamma_F} F \delta u d\Gamma = 0 \quad (30)$$

where \bar{u} is the prescribed general function to impose on Γ_u and α is a diagonal matrix of penalty coefficients whose non-zero elements are usually very large numbers (among $10^6 - 10^{15}$, the value of 10^{10} being systematically used in the following examples).

4.1.2 Influence on the convergence. The first numerical tests will be performed on a closed-form solution of problem (4) proposed by Warburton [27] by using the Rayleigh method with deflection functions as the product of beam functions. In this way, one can only express the solution by a modal expansion close to the computational frequency and the exact solution is obtained with an infinite number of eigenmodes. It is however possible to find an analytical solution of the following problem. Consider a plate of dimensions:

$$\Omega \equiv [0, x_{\max}] \times [0, y_{\max}] \quad \text{with} \quad x_{\max} = \frac{m\pi}{k_x} \quad \text{and} \quad y_{\max} = \frac{n\pi}{k_y} \quad (31)$$

where m and n are the values defining the number of waves along the x - and y -axis respectively, and k_x and k_y are defined in (10) with θ constant.

Associate the following the boundary conditions (B.C.)

$$\text{B.C. on } w : \begin{cases} x = 0 \Rightarrow w = 0 \\ y = 0 \Rightarrow w = 0 \\ x = x_{\max} \Rightarrow w = 0 \\ y = y_{\max} \Rightarrow w = 0 \end{cases} \quad (32)$$

$$\text{B.C. on } \beta_x : \begin{cases} x = 0 \Rightarrow \beta_x = k_x \sin(k_y y) \\ y = 0 \Rightarrow \beta_x = 0 \\ x = x_{\max} \Rightarrow \beta_x = k_x \cos(k_x x_{\max}) \sin(k_y y) \\ y = y_{\max} \Rightarrow \beta_x = 0 \end{cases} \quad (33)$$

$$\text{B.C. on } \beta_y : \begin{cases} x = 0 \Rightarrow \beta_y = 0 \\ y = 0 \Rightarrow \beta_y = k_y \sin(k_x x) \\ x = x_{\max} \Rightarrow \beta_y = 0 \\ y = y_{\max} \Rightarrow \beta_y = k_y \sin(k_x x) \cos(k_y y_{\max}) \end{cases} \quad (34)$$

The problem has the very simple following solution

$$w^{ex}(x, y) = \sin(k_x x) \sin(k_y y) \quad (35)$$

$$\begin{cases} \beta_x^{ex}(x, y) = \frac{\partial w^{ex}(x, y)}{\partial x} = k_x \cos(k_x x) \sin(k_y y) \\ \beta_y^{ex}(x, y) = \frac{\partial w^{ex}(x, y)}{\partial y} = k_y \sin(k_x x) \cos(k_y y) \end{cases} \quad (36)$$

Figures 9(a-c) represent the fields w , β_x and β_y for $m = n = 4$ and $\theta = 45^\circ$.

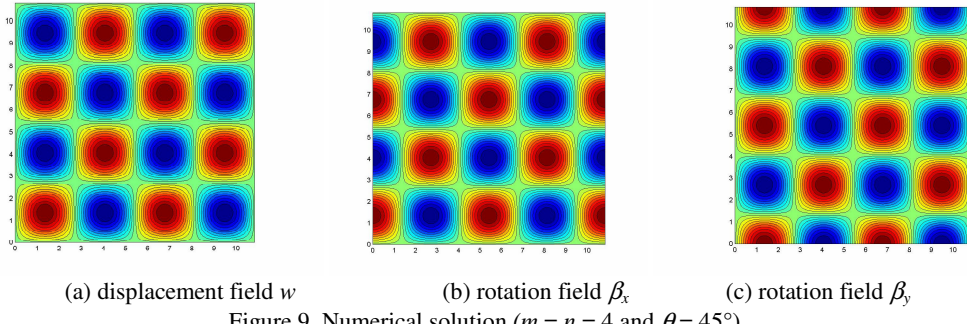


Figure 9. Numerical solution ($m = n = 4$ and $\theta = 45^\circ$).

For the comparison, different convergence curves are presented, corresponding to two different choices of basis (one polynomial basis and one basis containing the exact terms for two propagation angles), and also to different boundary conditions handling.

The following methods are compared :

- PUM with a polynomial basis (order 3 for the deflection and order 2 for the rotations)
 - B.C. with linear variations on the edges (*PUMpoly - B.C. lin*)
 - B.C. using the penalty method (*PUMpoly - B.C. pen*)
- PUM with exact basis (with 2 propagation angles)
 - B.C. imposed with a number x of Lagrange multipliers between 2 nodes (*PUMexact - B.C. Lagr-x*)
 - B.C. using the penalty method (*PUMexact - B.C. pen*)

Figures 10 (a-b) show the convergence (using a uniform refinement of the mesh) of these methods for a plate with $m = n = 2$ and $\theta = 60^\circ$ and for a plate with $m = n = 4$ and $\theta = 45^\circ$ respectively.

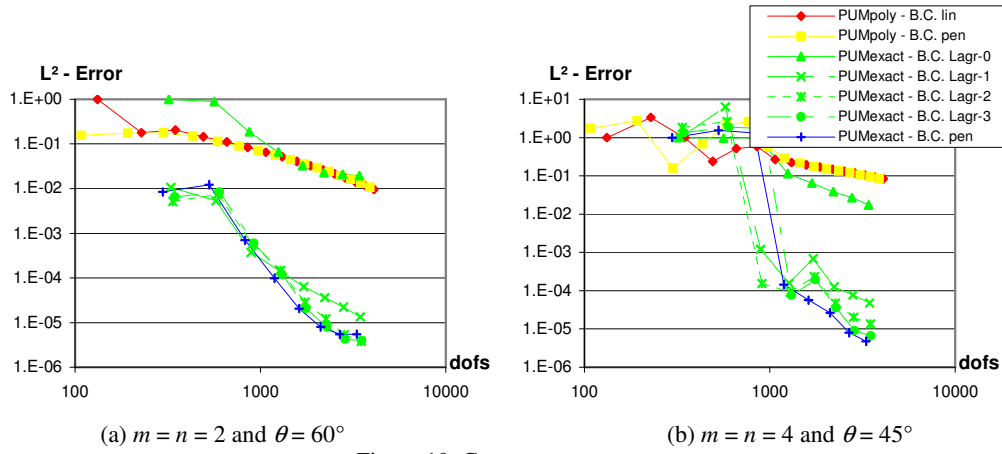
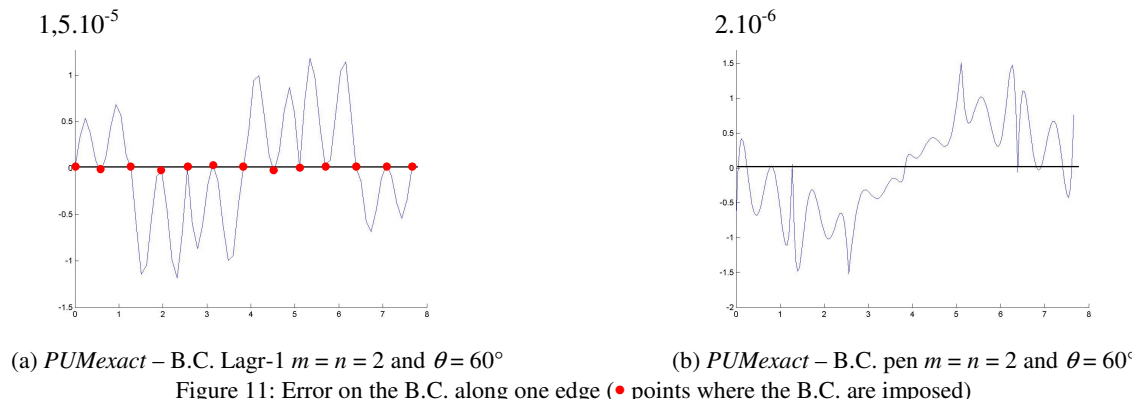


Figure 10. Convergence curves

Using linear variational boundary conditions or a penalty method to impose the boundary conditions for the PUM with polynomial bases provides nearly the same convergence curves (see *PUMpoly - B.C. lin* and *PUMpoly - B.C. pen*). For a polynomial choice, boundary condition type of impositions does not affect the global error we obtain on the whole plate : the error on the boundary conditions is too small in comparison with the error on the whole domain. For a PUM with bases enriched by exact solution terms, the error on the boundary conditions affects the error on the plate deflection. Indeed, the solution obtained is more accurate if more Lagrange multipliers are used, and the best solution is obtained by using the penalty method. Next two figures 11(a-b) underline this behaviour. The error over the deflection is plotted on one edge of the plate for $m = n = 2$ and $\theta = 60^\circ$: with Lagrange multipliers the error on the B.C. is nearly equal to zero at the points where the multipliers are imposed, but in average, the error is greater than it is by using the penalty method.



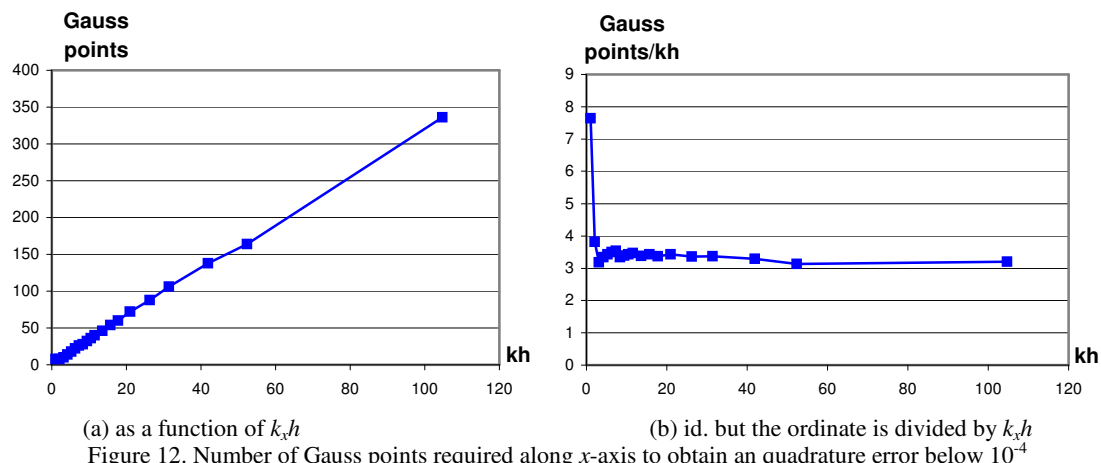
(a) *PUMexact - B.C. Lagr-1* $m = n = 2$ and $\theta = 60^\circ$

(b) *PUMexact - B.C. pen* $m = n = 2$ and $\theta = 60^\circ$

Figure 11: Error on the B.C. along one edge (● points where the B.C. are imposed)

4.2 Influence of the numerical integration with a Gauss quadrature

Integrals (20) and (21) have to be numerically computed. These integrals contain derivatives of shape functions and, for the proposed PUM formulation, the shape functions are constructed with harmonic terms. The evaluation of the integrals cannot be exact as is the case for integrals containing shape functions built from polynomial terms. It is well known that when the number of oscillations becomes important, many evaluation points are necessary in order to obtain an accurate integration: the higher the value $k_b h$, the higher the number of points of Gauss (where k_b is the wave number and h is the element average size). The next figures illustrate this: figure 12(a) presents the number of points of Gauss needed along the x -axis as a function of $k_x h$, and figure 12(b) represents the number of points of Gauss needed divided by $k_x h$ along the x -axis. The number of points of Gauss needed simply means that the solution has reached a L^2 -error of 10^{-4} .

(a) as a function of $k_x h$ (b) id. but the ordinate is divided by $k_x h$ Figure 12. Number of Gauss points required along x -axis to obtain an quadrature error below 10^{-4}

It is interesting to observe that the number of points of Gauss is nearly a linear function of the value $k_x h$: the slope can be found with figure 12(b) where the curve moves towards a constant equal to 3.2. Except for small values of $k_x h$, four points of Gauss per $k_x h$ are necessary to obtain accurate approximations.

5. NUMERICAL EXAMPLE

The numerical example considered is the free plate shaken at the corner as pictured in figure 8(a). The main criteria to assess the proposed method consists in the demonstration that :

- with coarse discretisations and few degrees of freedom, the method gives better approximations than a finite element modelling ;
- even if there are iterations, the new method is cheaper than the classical finite element when the frequency increases.

5.1 Convergence

The reference solution is the solution obtained with a PUM with polynomial bases and using 40 by 40 elements (20.172 degrees of freedom are used). By a simple extrapolation, the error in L^2 -norm of the reference at 780Hz is approximately about $5 \cdot 10^{-5}$ and at 1560Hz about $8.5 \cdot 10^{-4}$.

Figures 13(a-b) show the convergence of a classical finite element (ACTRAN® software), the convergence of the PUM using a polynomial basis (*PUMpoly*) and the convergence of the PUM using exact solution terms (3 angles of propagation for each discretisation) at 780 and 1560 Hz. The convergence curves are obtained by refining uniformly the mesh.

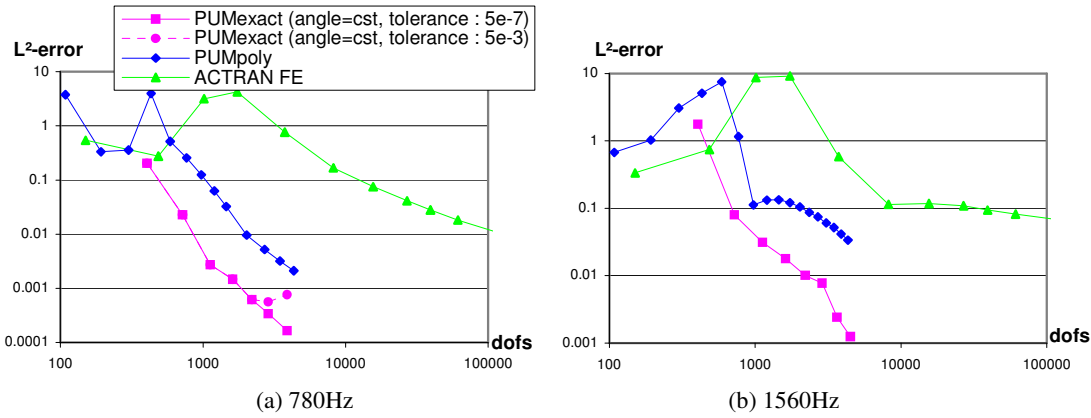


Figure 13. Convergence curves

We clearly observe better results when using a PUM with polynomial terms or containing terms from the exact solution. For the *PUMexact* solution, the number of angles of propagation is constant and is equal to 3; only the mesh is refined. If the prescribed tolerance used to determine if the solution has converged is not small enough, the error on the solution is governed by this tolerance (see figure 13a).

Next two figures 14 (a-b) present the same convergence curves except for the *PUMexact*. Now the discretisation remains the same (3×3) and the number of angles of propagation used for the approximation increases (leading to systems with more degrees of freedom).

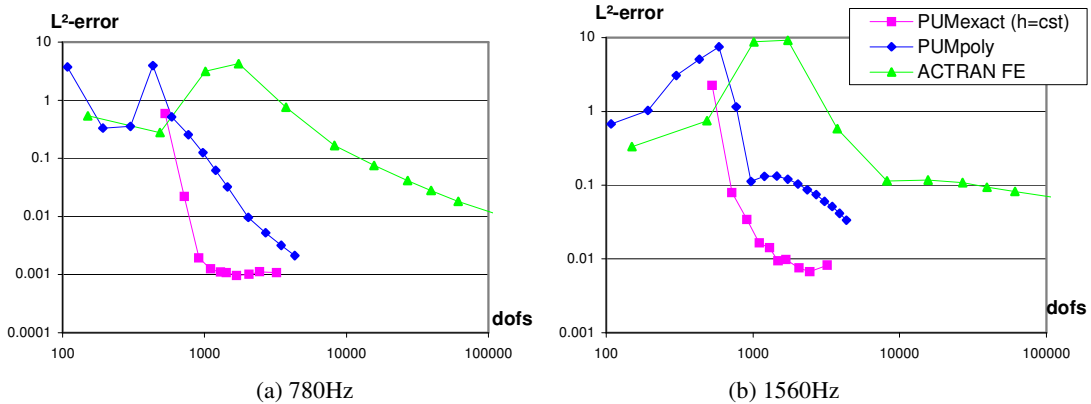


Figure 14. Convergence curves

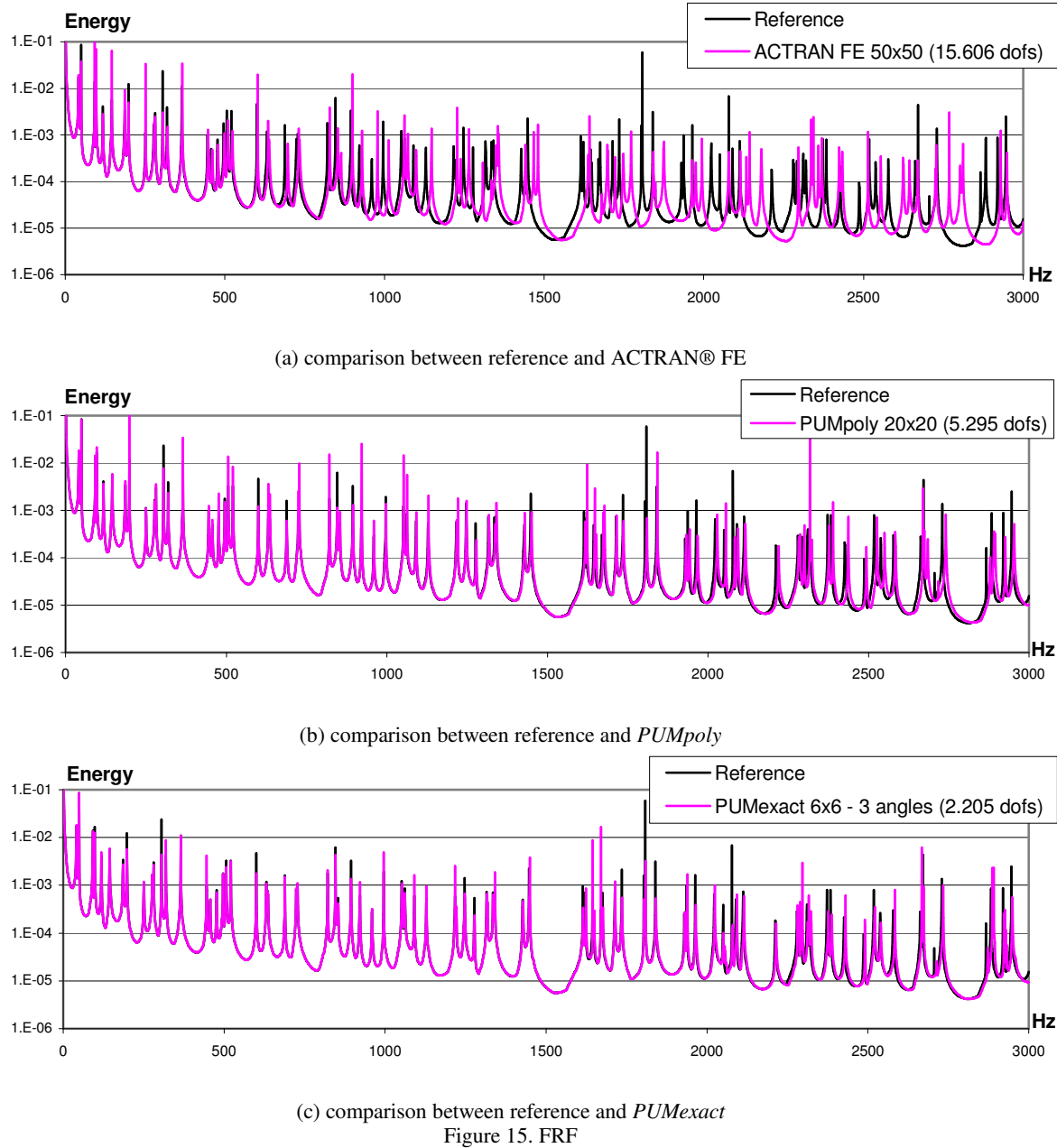
With a constant discretisation, it can be observed that the solution cannot be improved by adding terms in the basis with other propagation angles. As is described at the end of paragraph 3, the mesh has to be refined in order to better capture different propagation angles within the plate domain (it is the case for *PUMexact* in figures 13a and 13b).

In any case, the *PUMexact* solution gives accurate approximations for a same number of degrees of freedom in comparison with the *PUMpoly* solution and especially with the FE model.

5.2 Frequency analysis

Next three figures (15a, 15b and 15c) give the global energy of the plate as a function of the frequency. Because no damping is considered in the plate, peaks at the eigenfrequencies can be observed. On each graph, there are two curves. The first curve is for the reference solution computed with a mesh of 40 by 40 elements *PUMpoly* method (20,172 dofs). The second curve is for three different approximations respectively : the ACTRAN® FE with 50x50 elements, the *PUMpoly* with 20x20 elements and the *PUMexact* with 6x6 elements and three propagation angles.

On figure 15(a), we can see that the ACTRAN® FE curve no longer fits the reference curve above 1000Hz. On figure 15(b), the frequency limit for the *PUMpoly* solution is of about 2500Hz and on figure 15(c), we cannot distinguish the difference between the *PUMexact* approximation and the reference. It is interesting to note that the method providing the best results is also the method with the smallest number of degrees of freedom: only 2.205 dofs are sufficient whereas 15.606 dofs are not enough for the FE method.



There is however a major drawback using this new method. Indeed, for each frequency computation a new assembly of the matrices $[K]$ and $[M]$ (see equation 15) must be performed. The matrices $[K]$ and $[M]$ are frequency dependent when exact solution terms are incorporated in the PUM basis. Moreover, the *PUMexact* method requires some iterations to converge to the solution and at each iteration, propagation angles change, i.e. $[K]$ and $[M]$ matrices have to be computed again. When FRF's have to

be plotted, it is interesting to keep the propagation angles from the previous computation of the last frequency: the convergence over θ , and over w^h , is thus significantly improved.

For the *PUMpoly* FRF, it is like the FE method: only one assembly of the matrix is needed to obtain the whole response curve. In this case, *PUMpoly* method is a better choice than a FE one with respect to figures 15(a) and 15(b).

5.3 CPU-time analysis

The last discussion concerns the CPU-time analysis, and especially which method is recommended for the medium frequency range. For each method (FE, *PUMpoly* or *PUMexact*), when the frequency increases, the discretisation of the plate must be refined in order to obtain acceptable solutions. In a classical way, with FE, this refinement has a CPU-time cost that becomes very important for medium frequencies. Next figure 16 shows that the PUM is cheaper in comparison with the standard FE version.

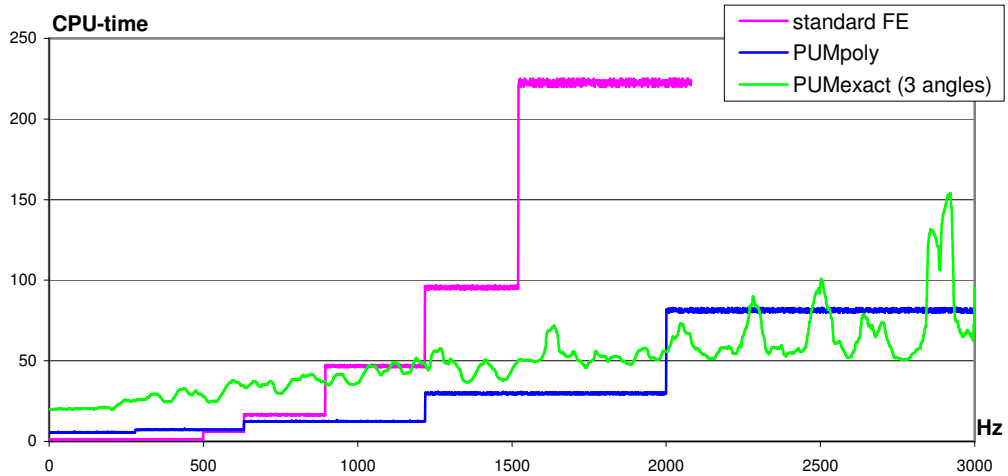


Figure 16 : CPU-time needed for each frequency to obtain an accurate approximation.

For the FE and the *PUMpoly* methods, the time resolution is constant by frequency bands: the CPU-time resolution only depends on the number of degrees of freedom, and a same discretisation is able to capture a good approximation until a certain frequency. Above this frequency, a refined mesh is required. For the *PUMexact* method, the mesh has to be refined too, but the time is also a function of the number of iterations. The number of iterations may be different for each frequency (reason of the chaotic aspect of the curve in figure 16).

In standard FE, an exponential behaviour for the CPU-time resolution has always been observed when the frequency increases. Here, the *PUMpoly* solution gives small resolution times in comparison with the FE method, but the curve also presents an exponential behaviour. In the case of the *PUMexact* solution, it is difficult to observe a specific type of behaviour but it can be said that, above 800Hz, the solution is cheaper than a FE one and, above 2000Hz, the solution is averagely cheaper than the *PUMpoly* approximation.

6. CONCLUSIONS

The new presented formulation uses a recent method, the Partition of Unity Method, enriched with special terms containing local information about the vibration of a plate. It seems to give very accurate results regarding its relatively coarse discretisation. Even if the resolution requires an iterative scheme, the method is still computationally less demanding than the standard FE or than the PUM using polynomial terms, when a solution in the medium frequency range has to be obtained. As this method is very promising, further works should be dedicated to assemble non coplanar plates, which is a necessary step before the extension of the method to 3D shells.

ACKNOWLEDGEMENT

Financial support of the first author is given by the Walloon Region (Belgium) under grant n° 9913937 (SIVA). The collaboration with the second author has been achieved thanks to a Belgian-French Tournesol grant.

REFERENCES

- [1] F. Ihlenburg, I. Babuška, 'Finite Element Solution of the Helmholtz Equation with High Wave Number. Part 1: The h-Version of the FEM'. *Comput. Math. Appl.* 1995, 38(9): 9-37.
- [2] Ph. Bouillard, F. Ihlenburg, 'Error estimation and adaptivity for the finite element solution in acoustics: 2D and 3D applications'. *Comput. Methods Appl. Mech. Eng.* 1999, 176(1-4): 147-163.
- [3] V. Decuvreur, Ph. Bouillard, A. Deraemaeker, P. Ladevèze, 'Validation of 2D Acoustic Models Based on the Error in Constitutive Relation'. *Journal of Sound and Vibration, available on-line*, 2004.
- [4] K. Gerdes, L. Demkowicz, 'Solution of the 3D Helmholtz equation in arbitrary exterior domains using hp-FEM and IFEM'. *Comput. Methods Appl. Mech. Eng.* 1996; 137: 239-273.
- [5] A. Côté, F. Charron, 'On the selection of p-version shape functions for plate vibration problems'. *Computers and Structures*. 2001; 79: 119-130.
- [6] T. Belytschko, Y. Y. Lu, L. Gu, 'Element-Free Galerkin Methods'. *Int. j. numer. methods eng.* 1994; 37: 229-256.
- [7] R. A. Uras, C. T. Chang, Y. Chen, W. K. Liu, 'Multiresolution Reproducing Kernel Particle Methods in Acoustics'. *Journal of Computational Acoustics*. 1997; 5(1): 71-94.
- [8] Th. E. Voth, Mark A. Christon, 'Discretization Errors Associated with Reproducing Kernel Methods: One-Dimensional Domains'. *Comput. Methods Appl. Mech. Eng.* 2001; 190(18-19): 2429-2446.
- [9] Ph. Bouillard, S. Suleau. 'Element-Free Galerkin solutions for Helmholtz problems: formulation and numerical assessment of the pollution effect'. *Comput. Methods Appl. Mech. Eng.* 1998; 162: 317-335
- [10] E. Chadwick, P. Bettes. 'Modelling of progressive short waves using wave envelopes'. *Int. j. numer. methods engrg.* 1997; 40: 3229-3245.
- [11] C. Farhat, I. Harari, L. P. Franca, 'The discontinuous enrichment method'. *Comput. Methods Appl. Mech. Eng.* 2001; 190: 6455-6479.
- [12] C. Farhat, I. Harari, U. Hetmaniuk, 'A discontinuous Galerkin method with Lagrange multipliers for the solution of Helmholtz problems in the mid-frequency regime'. *Comput. Methods Appl. Mech. Eng.* 2003; 192: 1389-1419.
- [13] I. Harari, C. Farhat, U. Hetmaniuk, 'Multiple-Stencil Dispersion analysis of the Lagrange multipliers in a Discontinuous Galerkin method for the Helmholtz equation'. *J. Comput. Acoustics*. 2003, 11(2):239-254.
- [14] W. Desmet, 'A wave based prediction technique for coupled vibro-acoustic analysis'. Ph.D. thesis, KU Leuven, division PMA, Leuven, 1998.
- [15] P. Ladevèze, L. Arnaud, P. Rouch, C. Blanzé, 'The variational theory of complex rays for the calculation of medium-frequency vibrations'. *Engineering Computations*. 2001; 18 (1/2): 193-214.
- [16] B. Van Hal, W. Desmet, D. Vandepitte, P. Sas, 'An efficient prediction technique for the steady-state dynamic analysis of flat plates'. *inter.noise 2000*, 29th International Congress and Exhibition on Noise Control Engineering, August 2000, Nice, France.
- [17] H. Riou, P. Ladevèze, P. Rouch, 'The variational theory of complex rays for medium-frequency vibrations of shells'. 2d MIT Conference on Computational Fluid and Solid Mechanics, Cambridge (USA), 2003, Elsevier.
- [18] Vanmaele, W. Desmet, D. Vandepitte, 'A wave based prediction technique for the steady-state dynamic analysis of three-dimensional plate structures'. ICSV10, Tenth International Congress on Sound and Vibrations, July 2003, Stockholm, Sweden.
- [19] P. Krysl, T. Belytschko, 'Analysis of thin plates by the element-free Galerkin method'. *Computational Mechanics*. 1995; 17 (1-2): 26-35.
- [20] Ph. Bouillard, V. Lacroix, E. De Bel, 'A meshless approach for 2D vibroacoustic problems'. *Revue européenne des éléments finis*. 2002, 11(7-8): 947-964.

- [21] E. De Bel, Ph. Bouillard, ‘An EFGM-PUM coupling for solving 2D vibro-acoustic problems in the mid-frequency domain’. ICSV10, Tenth International Congress on Sound and Vibrations, 2003, Stockholm, Sweden.
- [22] Ph. Bouillard, V. Lacroix, E. De Bel, ‘A wave oriented meshless formulation for acoustical and vibro-acoustical applications’. Journal of Wave Motion. 2004, 39(4): 295-305
- [23] I. Babuška, J. Melenk, ‘The partition of unity method’. Int. j. numer. methods engrg. 1997; 40: 727-758.
- [24] I. Babuška, Z. Zhang, ‘The partition of unity method for the elastically supported beam’. Comput. Methods Appl. Mech. Eng. 1998, 152(1-2): 1-18.
- [25] M. Gérardin, D. Rixen, ‘Théorie des vibrations : Application à la dynamique des structures’. Editions Masson, ISBN 2-225-83952-2, 1993.
- [26] K.Y. Dai, G.R. Liu, K. M. Lim, X.L. Chen, ‘A mesh-free method for static and free vibration analysis of shear deformable laminated composite plates’. Journal of Sound and Vibration 2004, 269:633-652.
- [27] Leissa, ‘Vibration of plates’. Acoustical Society of Amer. Publications, ISBN-1563962942, 1993.
- [28] T. Strouboulis, K. Copps, I. Babuška, ‘The generalized finite element method’. Comput. Methods Appl. Mech. Engrg., 190: 4081-4193, 2001.
- [29] T. Strouboulis, I. Babuška, K. Copps, ‘The design and analysis of the Generalized Finite Element Method’. Comput. Methods Appl. Mech. Engrg., 181: 43-69, 2000.
- [30] T. Strouboulis, K. Copps, I. Babuška, ‘The generalized finite element method: an example of its implementation and illustration of its performance’. Int. J. Numer. Meth. Engng., 47: 1401-1417, 2000.
- [31] I. Babuška, U. Banerjee, J. Osborn, ‘On principles for the selection of shape functions for the Generalized Finite Element Method’. Comput. Methods Appl. Mech. Engrg., 191: 5595-5629, 2002.

3.2 Couplage EFGM-PUM

Ce dernier paragraphe de la dissertation est destiné à montrer que nous disposons maintenant de tous les outils pour aborder la résolution du problème vibro-acoustique (fortement) couplé. L'équation discrétisée (1.11)

$$\begin{bmatrix} \mathbf{K}_S + j\omega \mathbf{C}_S - \omega^2 \mathbf{M}_S & \mathbf{K}_{sf} \\ \mathbf{K}_{fs} & \mathbf{K}_f + j\omega \mathbf{C}_f - \omega^2 \mathbf{M}_f \end{bmatrix} \begin{Bmatrix} \mathbf{u} \\ \mathbf{p} \end{Bmatrix} = \begin{Bmatrix} \mathbf{f} \\ \mathbf{0} \end{Bmatrix} \quad (3.11)$$

est résolue en considérant pour la partie solide les fonctions d'interpolation PUM (base polynomiale ou calculée), pour la partie fluide les fonctions EFGM (base polynomiale ou calculée), et pour les matrices couplées la multiplication des deux types de fonction.

$$\begin{aligned} \mathbf{K}_{sf} &= \int_{\Gamma} \{\mathbf{N}_{EFGM}\}^t \{\Phi_{PUM}\} d\Gamma \\ \mathbf{K}_{fs} &= \rho\omega^2 \mathbf{K}_{sf} \end{aligned} \quad (3.12)$$

Le couplage des deux méthodes ne présente donc aucune difficulté. L'article suivant contient une application à deux dimensions relative au couplage de la poutre de Timoshenko avec un domaine fluide 2D.

Une application 3D a été publiée par ailleurs dans [DEB04b]. Elle consiste en l'étude d'un dispositif expérimental composé d'une boîte en bois rigide et d'une plaque figurant la fenêtre latérale d'une voiture (Figure 3-1). Le dispositif est prévu pour subir un essai en soufflerie de manière à optimiser les propriétés visco-élastiques des vitres.

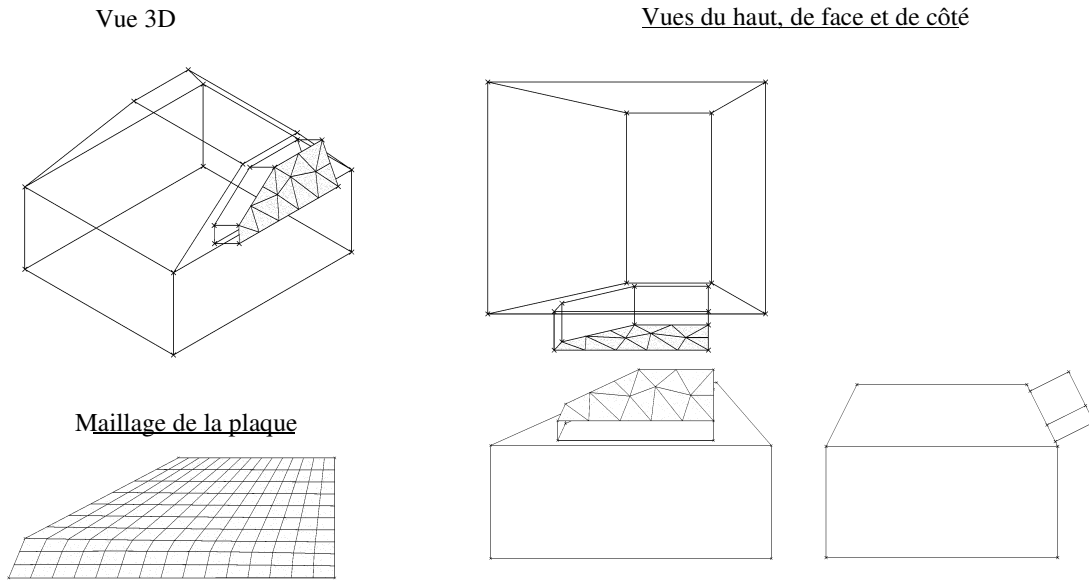


Figure 3-1. Dispositif expérimental. Boîte acoustique rigide excitée par la vibration d'une plaque.

Trois solutions numériques obtenues par des couplages différents sont comparées : une méthode éléments finis de degré 2 pour les domaines solide et fluide (notée *Actran* car calculée à l'aide du logiciel ACTRAN® au moyen d'éléments TET15-H20), une méthode EFGM à base linéaire couplée à une méthode PUM à base linéaire (notée *EFGM-PUMpoly*) et, enfin, une méthode EFGM à base linéaire pour le fluide couplée à une méthode PUM contenant des bases locales pré-calculées (notée *EFGM-PUMexact*). Les maillages utilisés sont décrits dans les Tables 3-1 à 3-3.

Maillage #	# ddl acoustiques	# ddl structure	# ddl	temps CPU (s)
1	884	3534	4418	122
2	3531	13359	16680	2979
3	7328	26259	33587	12361
4	7328	51909	59237	50229

Table 3-1. Nombre de degrés de libertés pour les différents maillages éléments finis (Actran TET15-H20). Temps CPU correspondant obtenu sur un ordinateur SunUltrasparc (900MHz) à l'aide du logiciel ACTRAN.

Maillage #	# ddl acoustiques	# ddl structure	# ddl	temps CPU (s)
1	781	240	1021	194
2	1694	576	2270	606
3	2998	576	3574	1443
4	6205	1056	7261	2620

Table 3-2. Nombre de degrés de liberté pour les différents maillages *EFGM-PUMpoly*. Temps CPU correspondant obtenu sur un ordinateur SunUltrasparc (900MHz) pour une implantation Matlab.

Maillage #	# ddl acoustiques	# ddl structure	# ddl	temps CPU (s)
1	781	900	1681	403
2	1694	2160	3854	1142
3(*)	6205	3960	10165	4397

Table 3-3. Nombre de degrés de liberté pour les différents maillages *EFGM-PUMexact*. Sur la base de nos résultats antérieurs [DEB04a], nous considérerons le maillage # 3(*) comme solution de référence. Temps CPU correspondant obtenu sur un ordinateur SunUltrasparc (900MHz) pour une implantation Matlab. Il s'agit d'une valeur moyenne pour la bande de fréquences [0-400](Hz) car la méthode requiert 2 à 7 itérations pour converger.

Procédons tout d'abord à une comparaison des courbes de réponse fréquentielles (FRF). Un point caractéristique est choisi dans la cavité et la pression (en dBA) est tracée en fonction de la fréquence dans les figures 3-2. Ces figures comparent les FRF pour des maillages comprenant un nombre de degrés de liberté à peu près identique.

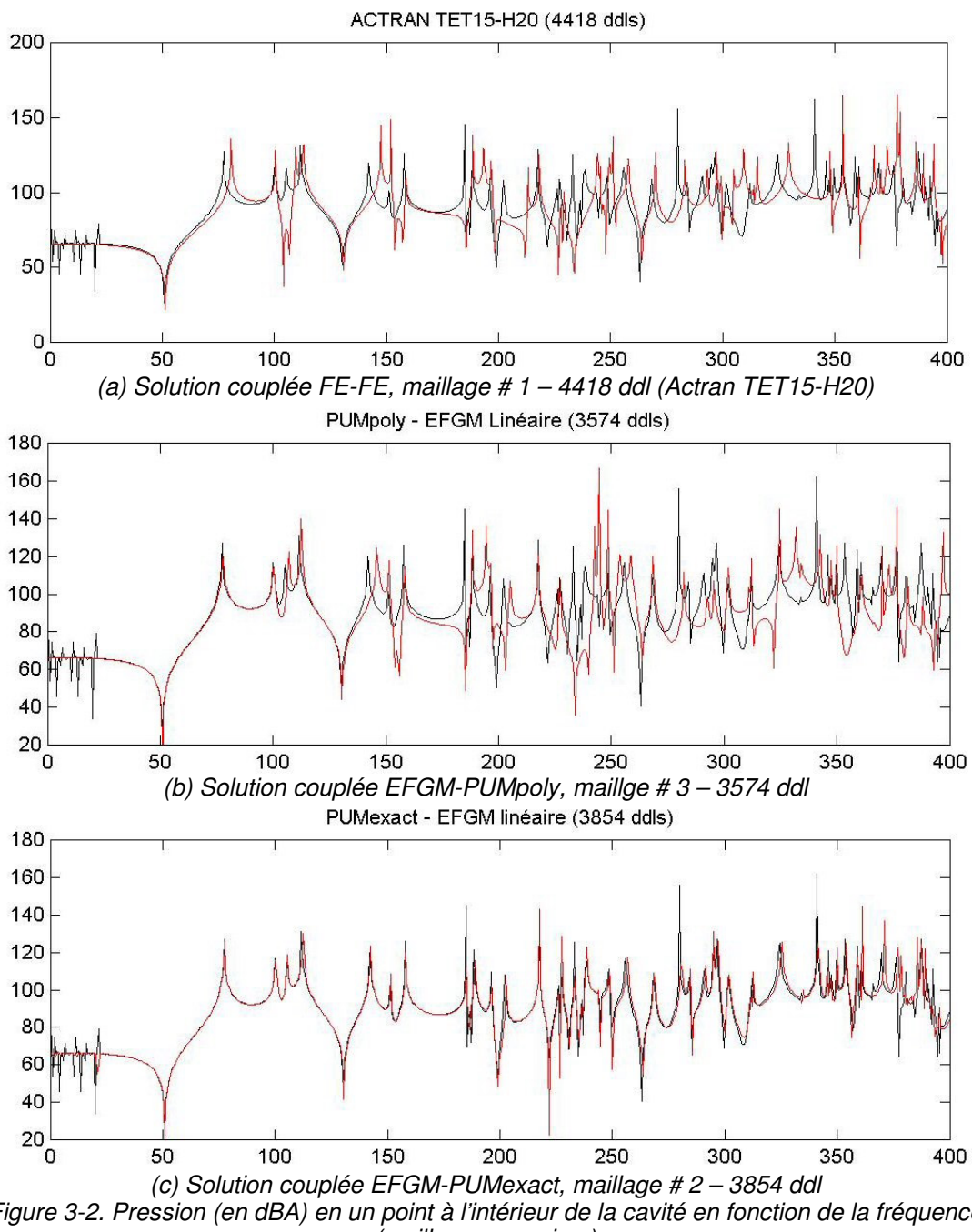


Figure 3-2. Pression (en dBA) en un point à l'intérieur de la cavité en fonction de la fréquence (maillages grossiers)

Dans chaque figure, la solution est tracée de même que la solution de référence (maillage #3 solution couplée *EFGM-PUMexact*). On peut voir dans la figure 3-2(a) que la solution éléments finis diffère déjà de la solution de référence en-dessous de 80 Hz, ce qui est très bas. Sur la figure 3-2(b), on peut voir que la solution couplée *EFGM-PUMpoly* est légèrement meilleure mais diffère de la solution de référence à partir de 145 Hz environ. Enfin, la figure 3-2(c) montre que la solution *EFGM-PUMexact* donne déjà une très bonne précision avec un maillage grossier. Ce dernier résultat montre une fois encore que la précision d'un problème couplé requiert une très bonne précision dans la partie structure.

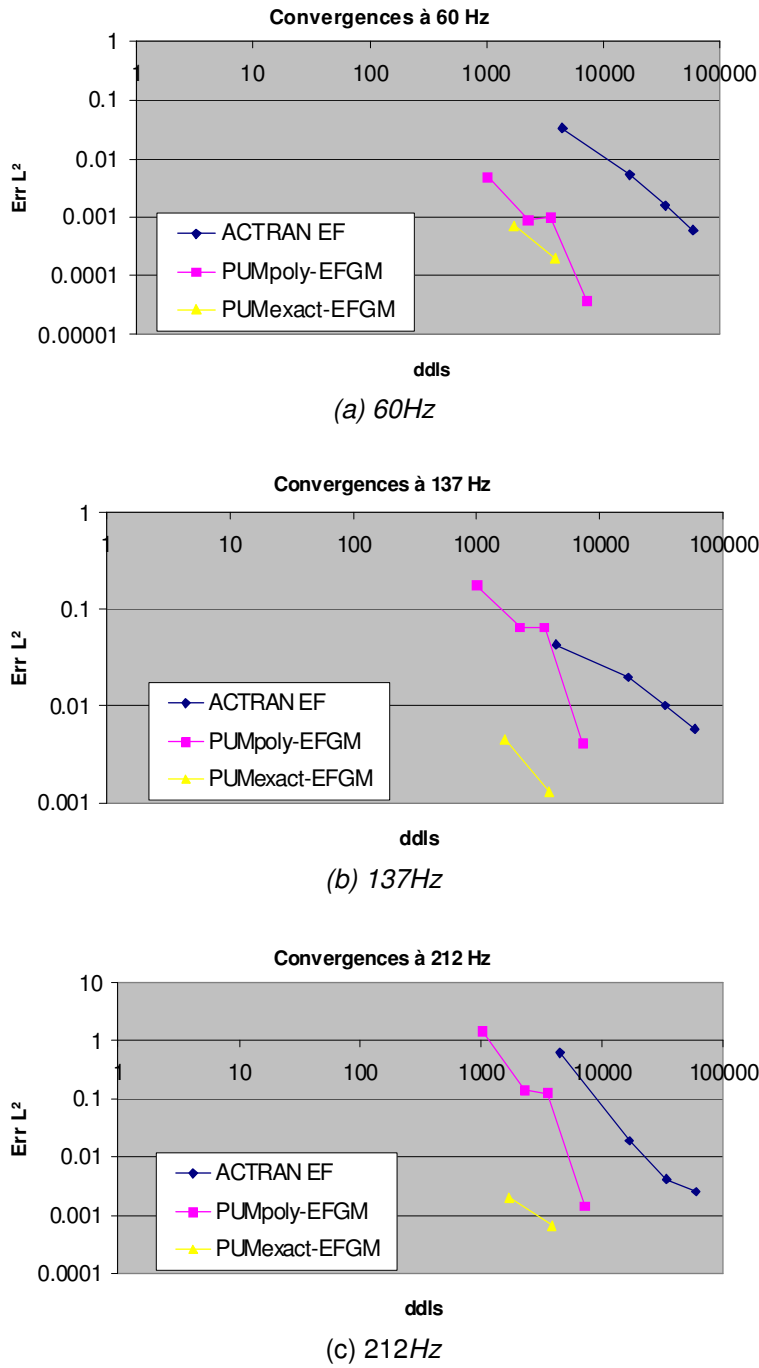


Figure 3-3. Courbe de convergence :
erreur sur la pression en norme L^2 en fonction du nombre de degrés de liberté.

Les figures 3-3(a-c) donnent les courbes de convergence (en norme L^2 sur la pression) pour les fréquences 60, 137 et 212 Hz. Ces courbes sont obtenues avec les maillages décrits dans les Tables 3-1 à 3-3 et ne sont pas parfaitement rectilignes car les maillages ne sont pas parfaitement hiérarchiques. Elles montrent à nouveau que la méthode EFGM-PUMpoly est nettement meilleure que les autres.

Enfin, les temps de calcul sont également comparés (voir Tables 3-1 à 3-3). On constate que les méthodes couplées EFGM-PUM(*poly* ou *exact*) sont intéressantes car elles permettent l'utilisation de maillages plus grossiers pour un même niveau de précision, ce qui implique un gain en temps de calcul.

L'article suivant est un reprint de Ph. Bouillard, V. Lacroix and E. De Bel, ‘A wave oriented meshless formulation for acoustical and vibro-acoustical applications’, J. Wave Motion 39/4 (2004) 295-305. Il rappelle la méthode EFGM pour l'acoustique et l'illustre sur une application 3D (source acoustique dans une boîte). Il expose ensuite la méthode PUM pour le calcul des vibrations et illustre le couplage à deux dimensions relatif au couplage de la poutre de Timoshenko avec un domaine fluide 2D.



Wave Motion 39/4 (2004) 295-305



A wave oriented meshless formulation for acoustical and vibro-acoustical applications

Ph. Bouillard*, V. Lacroix and E. De Bel

Department of Structural and Material Computational Mechanics, Université Libre de Bruxelles,
F.D. Roosevelt Av., 50, CP 194/5 – Brussels, Belgium

Received 3 December 2003

Abstract

Simulating acoustical or vibro-acoustical waves within the medium frequency range is still an open problem today. In this paper, we first demonstrate that it is possible to formulate an improved element-free Galerkin method (*I-EFGM*) for the uncoupled acoustical problem applied to three dimensional complex geometries. Then, we develop a partition of unity formulation extended for the elastodynamics (*PUM-dyn*). Finally, by coupling both formulations with an appropriate formulation for 2D vibroacoustical coupled problems, we demonstrate that an *I-EFGM* coupled to the *PUM-dyn* seems to be an excellent way to reach the medium frequencies accurately and with an acceptable CPU time.

Keywords : vibro-acoustics, meshless methods, dispersion error, medium frequencies

1. Introduction

Finite element (FEM) and boundary element (BEM) are still the most widely used methods to solve wave propagation problems, despite the considerable recent efforts to develop better suited numerical approaches. The key issue to improve the accuracy of the approximate numerical solution, or, alternatively, to simulate properly the medium frequencies, for wave propagation in bounded domains, or for near-field sub-domains in unbounded domains, is to control the dispersion error [1-3]. It is particularly crucial for industrial purpose which request robust methods for the medium frequencies within a reasonable computational cost, or sufficiently accurate numerical models for updating with experimental data [4]. The expression ‘medium frequencies’ actually depends on the context. Here, we are concerned with the noise inside cabins (cars, airplane, etc.). In this context, the expression ‘medium frequencies’ refers to 3 to 10 kHz throughout the paper.

Lots of numerical methods have been proposed to eliminate the dispersion, but none of them being totally ‘dispersion-free’. The first approaches were based on the idea of stabilizing the finite element method itself but they did not improve significantly the accuracy of the solution [5]. High order approximations were then proposed, based on the finite element method (*hp* formulations [6]) or on meshless methods [7-9]. But today, everybody seems to agree that it is even more advantageous to incorporate information on the solution itself into the numerical discrete subspace, see for instance the wave envelope approach [10] or the Discontinuous Galerkin FEM [11-13], or the Trefftz based approach

* Corresponding Author, Philippe.Bouillard@ulb.ac.be

[14]. Based on our previous work [15-16], we suggest to use, for the fluid domain, an improved Element-Free Galerkin Method (*I-EFGM*), and, for the solid domain, a generalized FEM based on the Partition of Unity Method formulated for the elastodynamics (*PUM-dyn*). This formulation aims to be general for any three-dimensional geometry addressing the coupled vibro-acoustical problem defined in a bounded or an unbounded domain.

This paper demonstrates that such a formulation allows us to reach accurately the medium frequencies for 3D uncoupled acoustical problems (Section 3) and for 2D coupled vibro-acoustical problems (Section 4). The numerical examples are related to car industries applications. The paper begins by addressing the problem of vibro-acoustics (Section 2).

2. Formulations for the vibro-acoustics

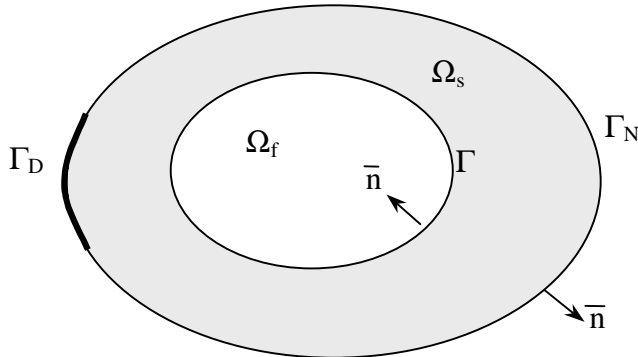


Fig. 1. A vibrating solid domain Ω_s is coupled to an acoustical fluid domain Ω_f

Consider an elastic solid domain Ω_s coupled with a fluid domain Ω_f along a wet surface Γ (Fig. 1). Within the solid, the displacements u_i are assumed to be small perturbations around a steady state. In a first approach, the structural damping and the body forces are neglected. In the fluid domain, the acoustical wave is assumed to propagate harmonically in a non viscous fluid without body forces around a steady state (linear acoustics). The acoustical damping is not considered yet. With these assumptions, the general formulation for the coupled vibro-acoustics is addressed by system of equations (1)

$$\begin{aligned}
 & \sigma_{ij,j}(u) + \rho_s \omega^2 u_i = 0 \quad \text{in } \Omega_s \quad (a) \\
 & \sigma_{ij}(u) n_j = \bar{F}_i \quad \text{on } \Gamma_N \quad (b) \\
 & u_i = \bar{u}_i \quad \text{on } \Gamma_D \quad (c) \\
 & \sigma_{ij}(u) n_j = -p n_i \quad \text{on } \Gamma \quad (d) \\
 & \frac{\partial p}{\partial n} = \rho_f \omega^2 u_i n_i \quad \text{on } \Gamma \quad (e) \\
 & \Delta p + \frac{\omega^2}{c^2} p = 0 \quad \text{in } \Omega_f \quad (f)
 \end{aligned} \tag{1}$$

where ρ_s and ρ_f denote the mass density of the solid and of the fluid respectively. Equation 1(a) is the elastodynamics classical equation, with its boundary conditions 1(c) on Γ_D (restraints) and 1(b) on Γ_N (traction). Equation 1(d) represents the loading of the pressure forces on the solid on Γ . Equation 1(e) represents the action of the structural vibrations on the fluid. If the structural velocities are given, the problem is said to be uncoupled or weakly coupled, and equation 1(e) is reduced to a Neumann boundary

condition for the fluid. Finally, equation 1(f) is the Helmholtz equation for the acoustic pressure p . Further information about fluid-structure interactions can be found in [17].

Whatever the approximation method, the discretisation of the variational form always leads to a linear system of equations of the form

$$\begin{bmatrix} K_s - \omega^2 M_s & K_{sf} \\ K_{fs} & K_f - \omega^2 M_f \end{bmatrix} \begin{Bmatrix} u \\ p \end{Bmatrix} = \begin{Bmatrix} f \\ 0 \end{Bmatrix} \quad (2)$$

where K_s and M_s are the solid stiffness and the solid mass matrices, K_f and M_f are the acoustical stiffness and the acoustical mass matrices, and K_{sf} and K_{fs} the coupling matrices. This formulation is not symmetrical but can be symmetrized [17].

3. Uncoupled acoustics in three dimensional bounded domains

3.1. Motivation

Most of real-life acoustical problems being three-dimensional, we investigate the possibilities of the meshless methods. Our first idea was to formulate an Element-Free Galerkin method (EFGM), first proposed by T. Belytschko for crack propagation [18], with polynomial bases. This formulation already gives a significant improvement of the accuracy (vs. the classical FEM solutions) coming from the non rational, or high order, shape functions that are better suited to approximate waves than polynomial terms [19]. Nevertheless, it was still limited to relatively low frequencies. Then, we decided to incorporate information on the solution into the basis of the subspace, first by putting a set of plane waves, second by defining a local basis based on a computed wave phase.

For the particular case of Helmholtz equation 1(f), we take advantage of the fact that the local basis of an Element-Free Galerkin method can naturally contain terms of \sin or \cos functions. Moreover, since the pressure is a complex variable, terms in $\cos\theta(x,y,z)$ and $\sin\theta(x,y,z)$ are introduced in the *meshless* basis, where $\theta(x,y,z)$ is the value of the phase of the pressure field in each point (x,y,z) of the domain. Since $\theta(x,y,z)$ is *a priori* unknown, it is first computed, for instance, with an EFGM with polynomial linear basis. Then, with the new θ -dependant local *meshless* basis, very accurate results are demonstrated on academic [15] or real-life 3D problems within a large frequency range (see paragraph 3.3).

3.2. The improved defect-correction EFGM (I-EFGM)

The complex pressure can always be written as

$$p(x,y) = \bar{P}(x,y) [\cos \theta(x,y) + j \sin \theta(x,y)] \quad (3)$$

where $\bar{P}(x,y)$ is the amplitude of the wave and $\theta(x,y)$ its phase. Therefore, if the phase is exactly known over the whole domain, then the approximate pressure p^h can be *exactly* computed considering an expansion

$$p^h(x) = \mathbf{P}^t(x) \mathbf{a}(x) \quad (4)$$

with the basis

$$\mathbf{P}^t(x,y) = \{\cos \theta(x,y), \sin \theta(x,y)\} \quad (5)$$

where the unknown coefficients $\mathbf{a}(x)$ are fixed in an EFGM manner by using a moving least square approximation [18].

Obviously, for real-life cases, the distribution of $\theta(x,y)$ is *a priori* unknown. Thus, in the latter, $\theta(x,y)$ will be approximated by a distribution $\theta^h(x,y)$ obtained by a first computation of the pressure field using, for instance, a linear polynomial *meshless* basis

$$\mathbf{P}^t(x,y) = \{1, x, y\} \quad (6)$$

With this basis, a first approximation of the pressure $p_I^h(x,y)$ and of the phase $\theta_I^h(x,y)$ is computed. Then, the basis defined by

$$\mathbf{P}^t(x,y) = \{1, \cos \theta_I^h(x,y), \sin \theta_I^h(x,y)\} \quad (7)$$

is considered with $\cos \theta_I^h(x,y)$ and $\sin \theta_I^h(x,y)$ coming from the first computation. The monomial constant term is added to regularize the approximation. A new approximated pressure field $p_{II}^h(x,y)$ is computed. Of course, this method could be iterated: a third approximation of the pressure could be computed with a new basis of type (7) by using the second approximate solution $p_{II}^h(x,y)$ and so on until the correction on θ stands below a prescribed tolerance.

3.3. Numerical example

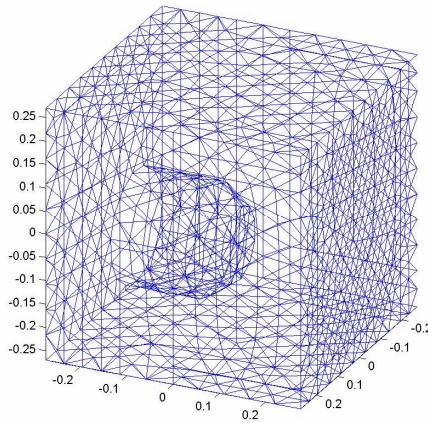


Fig. 2. Finite element mesh of the experimental set-up. The acoustical source is located close to a corner.

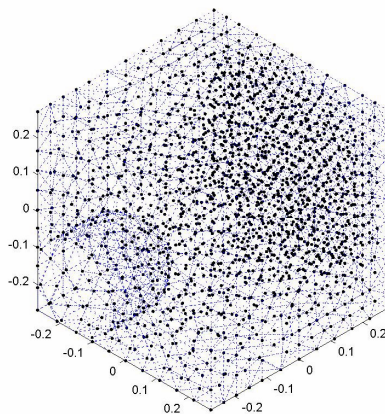


Fig. 3. I-EFGM distribution of nodes (identical to the FE nodes of fig. 2)

The numerical example is a three-dimensional experimental set-up developed to analyse the acoustical transparency of engine shields. The geometry is already complex because of the acoustical source located close to one corner of the box (see fig. 2).

The source will notably reduce the volume and one cannot consider the sound field to be diffuse, at least not below 1500Hz. The source is represented as a vibrating surface. The fluid is the air (mass density 1.225kg/m^3 , speed of sound 340m/s). Acoustical damping is introduced through a complex speed of sound ($c = 340 + 3.4j \text{ m/s}$). Fig. 3 gives the distribution of nodes used to perform the acoustical response. This distribution is taken identical to the finite element nodes (Fig. 2). Fig. 4 gives the acoustical Frequency Response Function – FRF - (without damping) in three points: at the center of the cavity, close to the source (baffle), and on the roof. One can see the strong difference between these curves due to the relatively small volume of the cavity. Methods based on plane wave assumption, or analytical functions, would fail to capture such a difference.

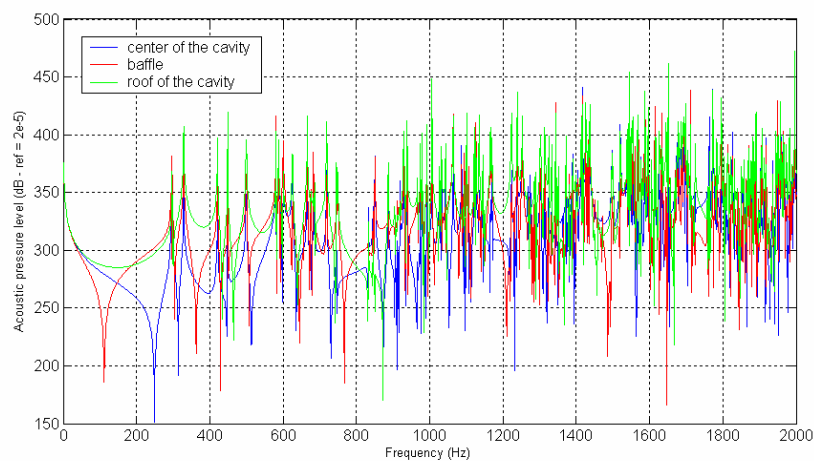


Fig. 4. Frequency Response Function (FRF) at (a) the center of the cavity (b) close to the source (c) on the roof.

Fig. 5(a-c) show the acoustical pressure normalized level at 314Hz, 446Hz, 513Hz respectively. These figures allow us to understand the important difference between the FRF curves in the different location given in fig. 4.

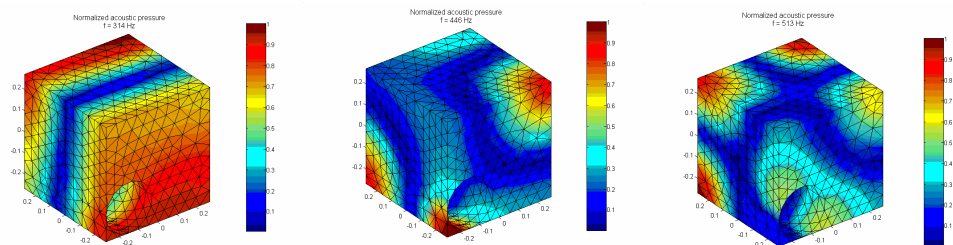
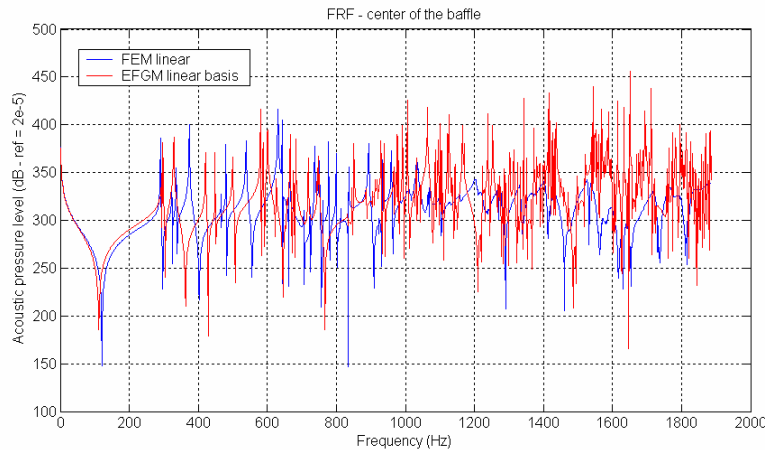


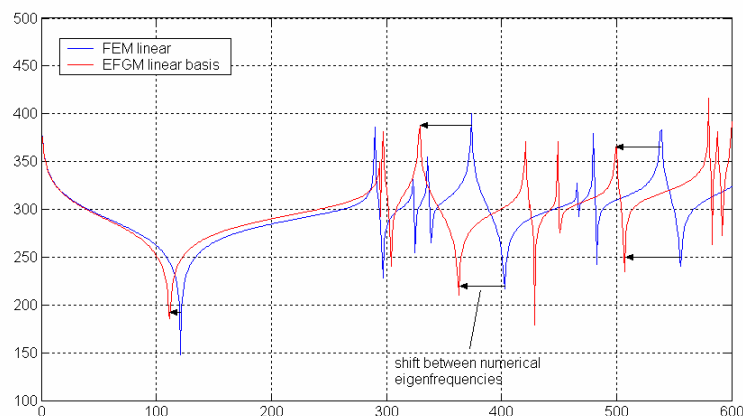
Fig. 5. Acoustical normalized pressure distribution at

Fig. 6(a) gives the FRF curve at the centre of the baffle for the [0-1500](Hz) frequency range. It compares the linear finite element solution to the first iterate Element-free Galerkin solution (with a linear basis only). The finite element mesh (fig. 2) has 1962 nodes with a mean meshsize $h=0.068m$. The classical rule of the thumb stating the a wave must be discretized by six (linear) elements gives a frequency limit of 833Hz. Fig. 6(b) shows that even for the low frequencies, below the rule of the thumb limit, the *I-EFGM* solution is much more accurate than the finite element one for the same distribution of nodes (and the same meshsize). For higher frequencies, it is known that there exists a limit above which the finite element wave is numerically damped [3]. In this case, the limit is 1443Hz. Fig. 6(c) shows that

the Element-free Galerkin solution, with only the first iterate (linear basis, eq. 6) already gives non damping results for the medium frequencies. Next iterates (eq. 7) would give still more accurate solutions.



*Fig. 6(a). FRF response at the center of the baffle.
Comparison between linear finite element and linear EFGM solution.*



*Fig. 6(b). FRF response at the center of the baffle.
Comparison between linear finite element and linear EFGM solution: zoom on the low frequencies.*

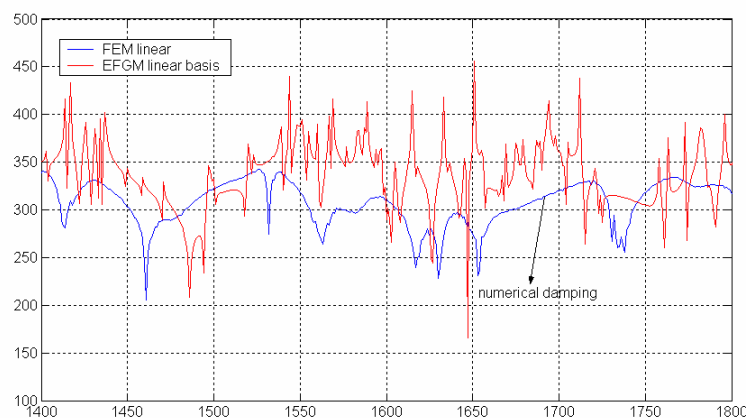


*Fig. 6(c). FRF response at the center of the baffle.
Comparison between linear finite element and linear EFGM solution: zoom on the medium frequencies.*

4. Coupled vibro-acoustics in two-dimensional bounded domains

4.1. Motivation

The motivation to develop a meshless solution for the elastodynamic problem is based on the same reasons than for the acoustic problem. Here again, a formulation able to capture the wave propagation phenomena, particularly for medium frequencies, is needed. However, since most of the real-life vibro-acoustic problems are three dimensional, it is necessary to formulate a method for the shell behaviour. Even if there have been some trials to formulate shell problems with EFGM (see e.g. [20]), it seems more efficient to keep the geometrical information of the shells with (finite) elements and, in the same time, to improve their formulation by taking advantage of the meshless solution. A very popular and easy way to achieve this is the Partition of Unity method, first proposed by I. Babuška [21].

The PUM can be seen as a generalized finite element method where the core ideas are, first, the construction of the spaces with local approximation properties and, second, the conformity of these spaces. In this paper, the PUM is formulated with a local enrichment of the basis derived from the exact solution of the elastodynamic problem. The terms of the exact solution of the homogeneous problem are introduced in the local basis everywhere since the pollution (dispersion) of wave propagation problem is global.

4.2. The Partition of Unity Method for elastodynamics (PUM-dyn)

Considering two-dimensional vibro-acoustical domains, i.e. a two-dimensional fluid domain surrounded by beams, the elastodynamical vibrations of 2D beams have to be solved. The exact solution of the fourth order differential equation for the transverse deflection w for a thick (Timoshenko) beam satisfies the following equation

$$w(x) = C_1 \sin\left(\alpha_1 \frac{x}{L}\right) + C_2 \cos\left(\alpha_1 \frac{x}{L}\right) + C_3 \sinh\left(\alpha_2 \frac{x}{L}\right) + C_4 \cosh\left(\alpha_2 \frac{x}{L}\right) \quad (8)$$

where α_i are non dimensional parameters function of the material and the geometrical properties of the beam and of the pulsation. These terms are used to define the approximate displacement field

$$w^h(x) = \sum_i N_i^w(x) \sum_j V_j^{w(i)}(x) a_{ij}^w = \sum_i \{\Phi_i^w\}^t \{A_i^w\} \quad (9)$$

where $\{\Phi_i\} = \{N_i V_1^{(i)} \dots N_i V_m^{(i)}\}$ and $\{A_i\} = \{a_{i1} \dots a_{im}\}$ (m is the number of functions in the basis). According to equation (8), the basis contains $\{\sin, \cos, \sinh, \cosh\}$ functions. The same developments can be done for the longitudinal displacement u ($\{\sin, \cos\}$ functions) and for the rotation θ ($\{\sin, \cos, \sinh, \cosh\}$ functions). Exactly in the same fashion as for acoustical computations, a significant improvement can be reached if the local propagation angle is computed by a first computation, with polynomial subspace for instance. The formulation, detailed in [22], is adapted for the beams and the plates.

4.3. The coupled I-EFGM / PUM-dyn formulation

To compute the matrices K_{sf} and K_{fs} in equation (2) we need to couple the pressure p with the transversal displacement w . The coupling leads to the following matrices

$$\begin{aligned} K_{sf} &= \int_{\Gamma} \{\bar{N}\}^t \{\Phi\} dS \\ K_{fs} &= \rho \omega^2 K_{sf} \end{aligned} \quad (10)$$

4.4. Numerical example

In this section, a recent benchmark proposed in [14] is presented. In fig. 7(a), the geometry is given. It consists of an acoustical cavity filled with air ($\rho_a = 1.225 \text{ kg/m}^3$, $c = 340 \text{ m/s}$), surrounded by rigid walls except for the upper wall, where the cavity is coupled to a 2mm thick aluminum plate ($E = 70 \text{ GPa}$, $\nu = 0.3$, $\rho_s = 2790 \text{ kg/m}^3$). The plate is excited by a unit force (see fig. 7a).

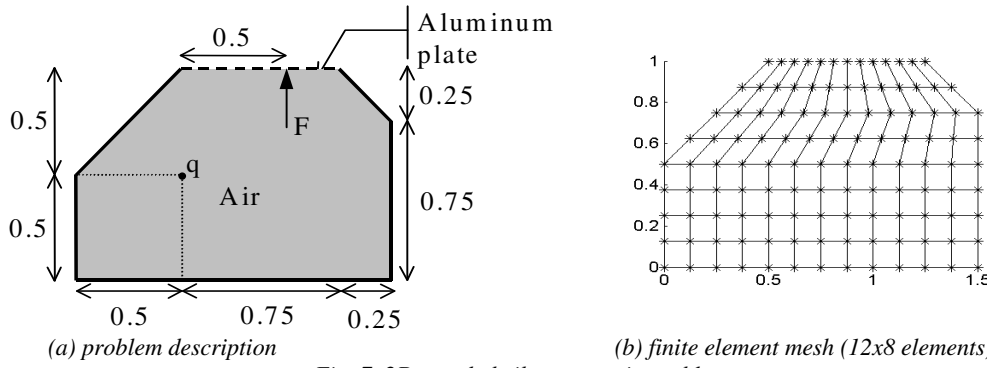


Fig. 7. 2D coupled vibro-acoustic problem

For this benchmark, coupled *FE/FE*, coupled *FE/I-EFGM* and coupled *PUM-dyn/I-EFGM* solutions are compared. An example of 12x8 finite element mesh is given in fig. 7(b). The nodes of the *I-EFGM* discretisation are chosen identical to the finite element nodes. Moreover, a reference solution is computed with a coupled *FE-FE* mesh of 62307 dof's (300x200 elements).

4.4.1. Error distributions

Results are given in terms of error in L^2 norm compared to the referenced solution. Fig. 8(a-c) give the local error distributions with a mesh of 24x16 elements using a *FE/FE*, *FE/I-EFGM* and *PUM-dyn/I-EFGM* coupling respectively (at 200Hz). For a quasi identical number of degrees of freedom the *PUM-dyn/I-EFGM* method gives outstanding results in comparison with the *FE-FE* and *FE-EFGM* methods. Note that with a *FE/I-EFGM* choice, the advantage of a meshless solution in the fluid is lost because of the dominant error in the *FE* structural solution.

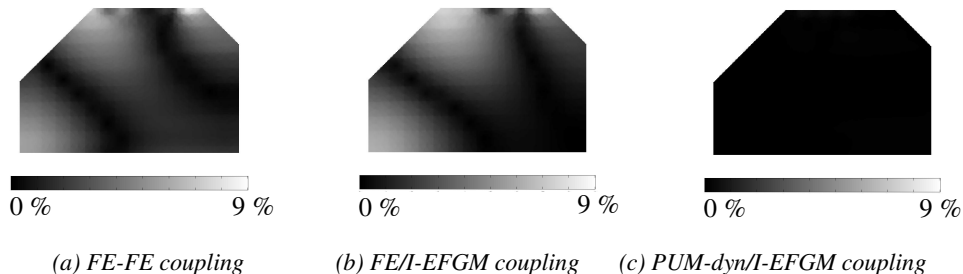


Fig. 8. Distribution of local errors at 200Hz

4.4.2 Convergence

A study of the convergence of the three different methods is also presented. Convergence curves are compared for three frequencies : at 200 Hz (between the 6th and 7th mode, fig. 9a), at 650 Hz (between the 27th and 28th mode, fig. 9b) and the last one at 930 Hz (between the 47th and 48th mode, fig. 9c).

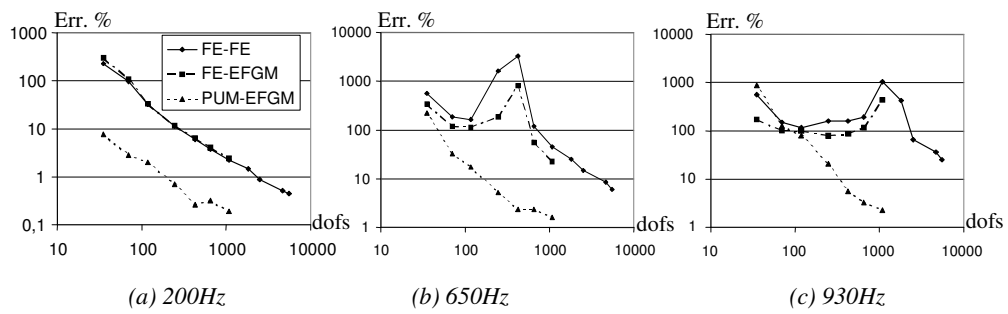


Fig. 9. Convergence curve for the coupled FE/FE, FE/I-EFGM, PUM-dyn/I-EFGM solution respectively.

Two important ideas emerge. First, the order of convergence is approximately the same (all the methods are with linear basis) but, for a same discretisation, the *PUM-dyn/I-EFGM* coupling provides more accurate solutions. Secondly, the *FE/I-EFGM* curve has nearly the same behavior than the *FE-FE* curve, showing that improving the solution in one domain only, is surely not a solution to reach the medium frequency range.

4.4.3 Frequency analysis

The next two figures give FRF at point *q* of fig. 7(a). Fig. 10 is plotted for a *FE-FE* 24x16 discretisation and fig. 11 for a *PUM-dyn/I-EFGM* 24x16 discretisation. One can clearly see that the *FE-FE* curve is limited in frequency by the pollution effect (see [2], $k^3 h^2 = 1$ for instance gives a limit in frequency of 344 Hz). With a same discretisation, the *PUM-dyn/I-EFGM* frequency limit is of about 1500 Hz (more than four times the *FE-FE* limit).

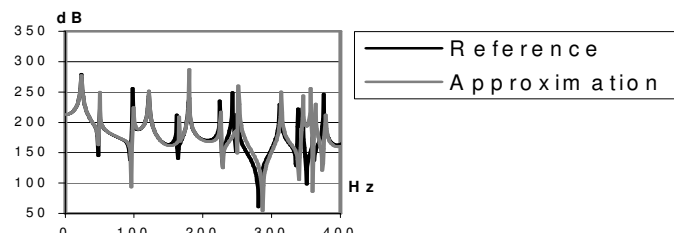


Fig. 10. FRF at point *q* (see fig. 7a) for a *FE-FE* 24x16 discretisation

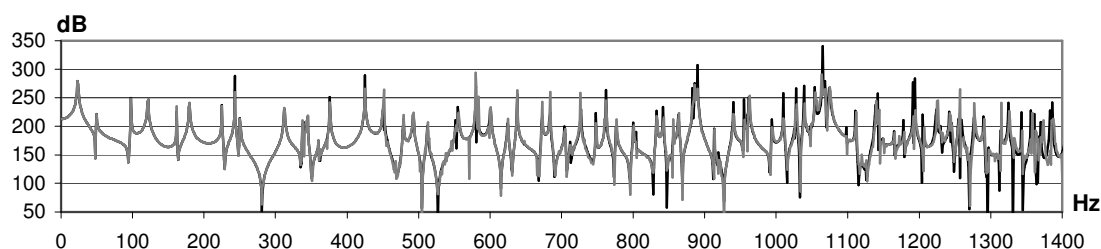


Fig. 11. FRF at point *q* for a *PUM-EFGM* 24x16 discretisation

4.4.4 CPU-time analysis

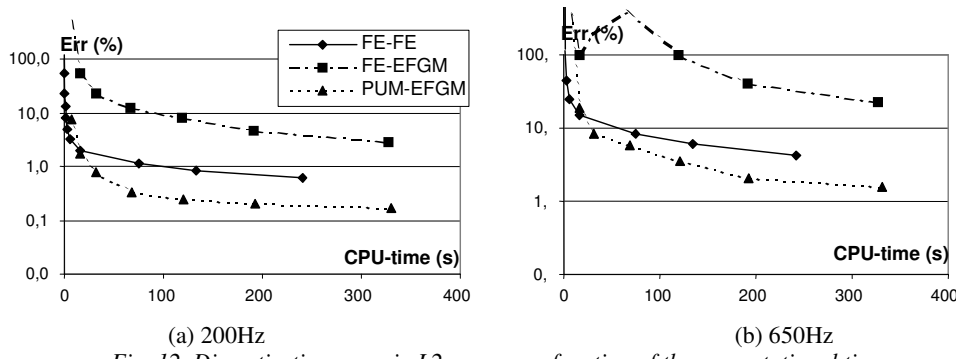


Fig. 12. Discretization error in L^2 norm as a function of the computational time.

The last discussion concerns the CPU-time analysis. Here, we consider that the best choice of coupling for a same level of accuracy is the one that gives the minimal CPU-time. Thus, in fig. 12(a-b), the error at 200 and at 650 Hz versus the CPU-time are presented. These results show that the worst choice is the *FE-EFGM* one, which shows bad errors for long computation times, and that the best choice is the *PUM-dyn/I-EFGM* where relatively small error in a reasonable time is obtained.

5. Conclusions

The paper presents a coupled improved Element-Free Galerkin Method/Partition of Unity Method formulation to solve accurately and efficiently the 3D acoustical and the 2D vibro-acoustical problems. Within the fluid, the improved EFGM, based on a defect-correction of the phase within a local basis, already gives very accurate results, for arbitrary three-dimensional geometries. Within the solid, the proposed PUM is an extension of the PUM for the elastodynamics, also with a two step computations. Further work will be dedicated to fully three-dimensional problems and to the development of an appropriate shell formulation.

Acknowledgements

Second and third authors are supported by the Région wallonne under grant “SIVA”. The authors would like to thank Prof. P. Villon (Université de Technologie de Compiègne, France) for the fruitful discussions.

References

- [1] F. Ihlenburg, I. Babuška, ‘Finite Element Solution of the Helmholtz Equation with High Wave Number. Part 1: The h-Version of the FEM’. *Comput. Math. Applic.* 1995, 38(9): 9-37.
- [2] Ph. Bouillard, F. Ihlenburg, ‘Error estimation and adaptivity for the finite element solution in acoustics: 2D and 3D applications’. *Comput. Methods Appl. Mech. Eng.* 1999, 176(1-4): 147-163.
- [3] Harari, ‘Finite element dispersion of cylindrical and spherical acoustic waves’. *Comput. Methods Appl. Mech. Eng.* 2001, 190(20-21): 2533-2542.
- [4] V. Decouvreur, Ph. Bouillard, A. Deraemaeker, P. Ladevèze , ‘Validation of 2D Acoustic Models Based on the Error in Constitutive Relation’, *Journal of Sound and Vibration*. 2003, accepted.
- [5] A. Deraemaeker, I. Babuška, Ph. Bouillard, ‘Dispersion and pollution of the FEM solution for the Helmholtz equation in one, two and three dimensions’. *Int. j. numer. methods eng.* 1999, 46:471-500.
- [6] K. Gerdes, L. Demkowicz, ‘Solution of the 3D Helmholtz equation in arbitrary exterior domains using hp-FEM and IFEM’. *Comput. Methods Appl. Mech. Eng.* 1996; 137: 239-273.
- [7] R. A. Uras, C. T. Chang, Y. Chen, W. K. Liu, ‘Multiresolution Reproducing Kernel Particle Methods in Acoustics’. *Journal of Computational Acoustics*. 1997; 5(1): 71-94.
- [8] Th. E. Voth, Mark A. Christon, ‘Discretization Errors Associated with Reproducing Kernel Methods: One-Dimensional Domains’. *Comput. Methods Appl. Mech. Eng.* 2001; 190(18-19): 2429-2446.

- [9] Ph. Bouillard, S. Suleau. ‘Element-Free Galerkin solutions for Helmholtz problems: formulation and numerical assessment of the pollution effect’. *Comput. Methods Appl. Mech. Eng.* 1998; 162: 317-335.
- [10] E. Chadwick, P. Bettes. ‘Modelling of progressive short waves using wave envelopes’. *Int. j. numer. methods eng.* 1997; 40: 3229-3245.
- [11] C. Farhat, I. Harari and L. P. Franca, ‘The discontinuous enrichment method’. *Comput. Methods Appl. Mech. Eng.* 2001; 190: 6455-6479.
- [12] C. Farhat, I. Harari and U. Hetmaniuk, ‘A discontinuous Galerkin method with Lagrange multipliers for the solution of Helmholtz problems in the mid-frequency regime’. *Comput. Methods Appl. Mech. Eng.* 2003; 192: 1389-1419.
- [13] I. Harari, C. Farhat and U. Hetmaniuk, ‘Multiple-Stencil Dispersion analysis of the Lagrange multipliers in a Discontinuous Galerkin method for the Helmholtz equation’. *J. Comput. Acoustics.* 2003, 11(2):239-254.
- [14] W. Desmet, B. van Hal, P. Sas, D. Vandepitte ‘A computationally efficient prediction technique for the steady-state dynamics analysis of coupled vibro-acoustic systems’, *Advances in Engineering Software.* 2002, 33:527-540.
- [15] Ph. Bouillard, V. Lacroix, E. De Bel, ‘A meshless approach for 2D vibroacoustic problems’, *Revue européenne des éléments finis.* 2002, 11(7-8): 947-964.
- [16] V. Lacroix, Ph. Bouillard, P. Villon, ‘An iterative defect-correction type meshless method for acoustics’, *Int. j. numer. methods eng.* 2003, 57(15): 2131-2146.
- [17] P. Morand, R. Ohayon, ‘Fluid-Structure Interaction’, John Wiley and Sons Ltd, Chichester, England, 1995.
- [18] T. Belytschko, Y. Y. Lu, L. Gu, ‘Element-Free Galerkin Methods’, *Int. j. numer. methods eng.*, 1994; 37: 229-256.
- [19] S. Suleau, A. Deraemaeker, Ph. Bouillard, ‘Dispersion and Pollution of Meshless Solutions for the Helmholtz Equation’. *Comput. Methods Appl. Mech. Eng.* 2000, 190(5-7): 639-657.
- [20] W. Kanok-Nukulchai, W. J. Barry, K. Saran-Yasoontorn, Ph. Bouillard, ‘On elimination of shear locking in the Element-Free Galerkin Method’, *Int. j. numer. methods eng.*, 2001 , 52(7): 705-725.
- [21] I.Babuška, J. Melenk. ‘The partition of unity method’. *Int. j. numer. methods eng.* 1997; 40: 727-758.
- [22] E. De Bel, P. Villon, Ph. Bouillard, ‘Forced vibrations in the medium frequency range solved by a partition of unity method with local information’, 2003, in preparation.